A Quest to Fluid Stress Tensor, Part I: Is Symmetric Stress Tensor Correct for Fluids?

Wanan Sheng [1,2]

[1] Department of Aerospace and Mechanical Engineering, South East Technological University, Carlow, R93 V960, Ireland
[2] SW MARE Technology Ireland
* Correspondence: wanan.sheng@setu.ie

Abstract: The symmetric stress tensor (SST) has been widely accepted in classical fluid mechanics for nearly two centuries, particularly following the work of Stokes in 1845. Its acceptance has been reinforced by the successful application of the Navier–Stokes equations to many practical flow problems. Nevertheless, the author has argued that certain interpretations of the SST lead to inconsistencies that warrant further examination. Establishing and communicating this argument has proved difficult, particularly because the proposed interpretation challenges a formulation routinely taught in fluid mechanics. Earlier attempts to publish these arguments encountered objections, including the absence of direct experimental measurements that distinguish the competing descriptions of the relevant stress components. For example, a tangential wall shear stress can be measured, whereas the corresponding transverse component invoked in the author's interpretation is not measured in the same manner. The present investigation therefore develops the argument through detailed examinations of familiar flow configurations, supported by a reported comparison between rotating water and rotating solid discs. The analysis considers six principal questions. First, in simple Couette flow, the author questions the interpretation of a transverse shear stress when the velocity has no component in that direction, relating this concern to the definition of a fluid as a material that deforms continuously under an applied shear stress. Second, the finite-element stress argument presented here is interpreted as implying uniform stresses under an imposed symmetry requirement, which would prevent the viscous force required in the momentum equations from being obtained. Third, conventional definitions of wall shear stress are examined to determine how the full stress tensor is represented in surface-force calculations. Fourth, the author's proposed inclusion of an additional transverse stress in the Stokes-flow calculation preserves the sphere's drag but produces a nonzero lift, contrary to the symmetry of the flow. Fifth, planar Poiseuille flow is used to examine an apparent conflict, within the proposed interpretation, between stress symmetry and the spatial increments required by differential calculus. Sixth, rigid rotation is examined to distinguish zero viscous dissipation from the transmission of mechanical energy under different loading conditions. A further discussion concerns the dissipation function for compressible flow under Stokes' hypothesis. These arguments are presented as the author's interpretation of the specified examples, rather than as experimentally established replacements for classical continuum mechanics. The purpose of the investigation is to clarify the physical meaning assigned to stress components and to encourage critical examination of the assumptions used in their construction. Comments on the derivations, their interpretation, and the experimental comparisons are welcomed.

Keywords: definition of a fluid, Newton's law of viscosity, fluid viscous stress tensor, symmetric viscous stress tensor, Navier–Stokes equation, planar Poiseuille flow, rigid-body rotation

Citation: Sheng, W. 2026. A Quest to Fluid Stress Tensor, Part I: Is Symmetric Stress Tensor Correct for Fluids? *TK Techforum Journal (ThyssenKrupp Techforum)* 2026(4): 1–33.
https://doi.org/10.71448/tk202641

Received: 01-Sep-2026
Revised: 02-Oct-2026
Accepted: 10-Oct-2026
Published: 07-Nov-2026

Copyright: © 2026 by the authors. Licensee TK Techforum Journal (ThyssenKrupp Techforum). This article is an open access article distributed under the terms and conditions of the Creative Commons Attribution (CC BY) license (https://creativecommons.org/licenses/by/4.0/).

1. Introduction

The development of the equations of fluid motion extended over many centuries, beginning with problems examined by ancient Greek scholars and continuing through the

establishment of classical mechanics. Newton's *Principia*, first published in 1687, provided an essential foundation for the subsequent formulation of fluid dynamics. According to Anderson [1], Newton devoted Book II of the *Principia*, entitled "Of the Motion of Bodies," to problems involving resistance and motion in fluids [2]. Despite this substantial contribution to fluid dynamics and hydrostatics, Newton encountered difficulties that had also challenged earlier investigators. One particularly influential contribution was his recognition of viscous resistance and the relationship between shear stress and velocity gradient. This relationship remains central to the description of Newtonian fluids and is commonly referred to as Newton's law of viscosity. The basic configuration and the associated velocity gradient are illustrated in Figure 1.

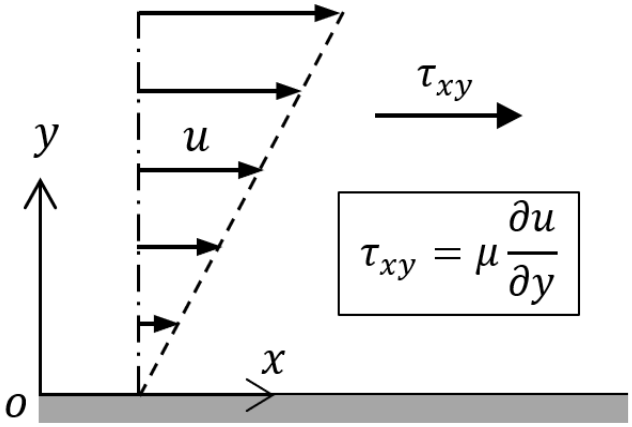


Figure 1. Shear stress and velocity gradient in Newton's law of viscosity.

A major advance in the mathematical description of fluid motion was made by Euler in 1755, with publication of the general differential equations following in 1757 [3]. Euler extended the application of Newton's second law from individual bodies to continuously distributed fluid motion. The formulation describes quantities at positions in space and is now known as the Eulerian approach. This contrasts with the Lagrangian description, which follows individual material particles and is also widely used in solid mechanics. Euler's equations and the associated development of Bernoulli-type relations provided a foundation for subsequent work on fluid motion. However, these equations did not include the viscous forces required to describe internal friction in a real fluid.

Subsequent developments concentrated on incorporating viscous forces into the differential equations of fluid motion. Historical accounts describe the successive formulations associated with Navier (1822), Cauchy (1823), Poisson (1829), Saint-Venant (1837), and Stokes (1845) as the first five developments of the viscous-flow equation [4–7]. Within this history, Cauchy's treatment extended principles of stress and momentum balance to fluids, whereas Stokes presented a derivation that closely resembles the treatment retained in many modern textbooks [8–14]. Masuda [6] discusses the use of the name Navier–Stokes by Prandtl in 1934. A comparison with Euler's equations shows that the central addition was the viscous force associated with internal fluid friction [5]. The precise constitutive representation of that force, and the interpretation of the stress components from which it is obtained, form the principal subject of the present investigation.

The early investigators and later scholars, including Maxwell, Kirchhoff, and Boltzmann, adopted a symmetric stress tensor in their treatments of fluid motion [6]. The subsequent success of the Navier–Stokes equations in practical applications strengthened the acceptance of this formulation. Nevertheless, the author's earlier study proposed that the same momentum equation could be derived using an asymmetric stress tensor (AST) [15]. That study also argued that an asymmetric formulation could address the interpretation of stress components in simple Couette flow. The present paper develops this line of argument through additional examples, with particular attention to the relationship

between the directions of stress components, the selected element faces, and the resulting velocity field.

Because the asymmetric stress tensor challenges the conventional use of the SST, the publication of the earlier study [15] was followed by a critique questioning its formulation and conclusions [16]. The present author disputes the formulas used in that critique; the detailed response is reserved for the subsequent study [17]. This disagreement concerns the mathematical representation and physical interpretation of fluid stresses, rather than merely a difference in notation. A related contribution by Luo [18] examines the conditions under which asymmetric stresses may arise in a fluid model. Its relevance is that stress symmetry should be considered together with the assumptions of the particular model, rather than treated independently of those assumptions.

Although the SST is the conventional formulation in classical fluid mechanics, alternative descriptions of viscous stress have been investigated historically, particularly during the 1960s [19–22]. Van D'en and Listrov [22], for example, discuss properties of asymmetric-fluid models, while Listrov [21] examines a viscous-fluid model with an antisymmetric stress contribution. These studies provide historical context for the present discussion, although their assumptions and additional degrees of freedom must be distinguished from those of an ordinary Newtonian fluid. During the late 1960s and early 1970s, developments in turbulence modelling and computer technology also accelerated the growth of computational fluid dynamics (CFD) [23–27]. CFD subsequently became a major means of investigating practical flows across a broad range of engineering applications [28–36]. Its success has increased the importance of understanding how the governing equations, constitutive assumptions, and numerical approximations interact. Mathematical investigations have continued alongside these computational developments. Ramm [37], for instance, presents a critical treatment of the Navier–Stokes problem. That author's conclusions are relevant to the debate considered here, but should not be equated with a general demonstration that analytical solutions are absent for all practical flow problems.

CFD has been highly successful as an approximate solution method for practical flow problems, but substantial challenges remain. The NASA CFD Vision 2030 report [38] identifies four grand-challenge applications: wall-resolved large-eddy simulation of complex industrial configurations; transient simulation of an off-design turbofan engine; multidisciplinary analysis and optimisation of a highly flexible advanced aircraft; and probabilistic analysis of a powered space-access configuration. These examples involve interacting difficulties in physical modelling, numerical resolution, computational cost, and the interpretation of simulation results. A related online discussion lists six broad challenges: high-performance computing, physical modelling of turbulence, numerical algorithms, geometry and grid generation, knowledge extraction, and multidisciplinary analysis and optimisation [39]. The two lists serve different purposes, but both indicate why continued examination of the governing assumptions remains useful. Detailed mathematical and physical studies can help clarify the meaning of computed quantities, identify the conditions under which a model is appropriate, and support a more careful interpretation of CFD predictions. The present investigation addresses the constitutive description of stress within that broader context.

The primary aim of this work is to examine the author's proposed inconsistencies in the conventional interpretation of the symmetric fluid stress tensor. The analysis focuses on familiar flow configurations so that the velocity field, stress components, and force contributions can be compared explicitly. It extends the earlier discussion of Couette flow [15] to planar Poiseuille flow, Stokes flow past a sphere, rigid rotation, and a particular compressible-flow deformation. Four principal arguments are considered. First, the author's application of the symmetry condition to stresses on a finite element is interpreted as producing a spatially uniform stress field, preventing the viscous-force increments required in the momentum equation. Second, the comparison of selected stress increments in planar Poiseuille flow is interpreted as a conflict between that symmetry construction and differential calculus. Third, the rigid-rotation examples distinguish the absence of relative sliding

from the question of whether torque and mechanical energy can be transmitted under an imposed load. Fourth, the compressible-flow calculation examines the zero dissipation obtained for a particular dilatational motion under Stokes' hypothesis. These examples are intended to make the proposed difficulties explicit enough to permit examination of each assumption and intermediate step. The corresponding asymmetric formulation is developed in the subsequent work [17], where the author proposes that it can resolve the issues raised here. The present paper concentrates on stating the arguments and comparing their consequences with the familiar flow descriptions.

The remaining sections follow the sequence of the argument. Section 2 introduces the general stress tensor, the corresponding momentum equations, and the conventional reasons for adopting a symmetric viscous stress tensor. It also reviews several ways of constructing the tensor and applying it in the Navier–Stokes equations. Section 3 examines the author's concerns about the interpretation of stress components in calculations of airfoil lift and drag. Section 4 then introduces planar Poiseuille flow as a simple configuration with an explicit velocity distribution and readily evaluated stress gradients. These expressions provide the basis for the proposed consistency tests in Section 5, including the author's arguments concerning spatially uniform stresses, grid dependence, and differential calculus. Section 6 considers the more detailed example of Stokes flow past a sphere and examines the nonzero lift obtained from the author's proposed additional surface-force contribution. Section 7 addresses rigid rotation, the reported comparison between water and solid discs, and a proposed pitch-filled cylinder arrangement for discussing torque transmission. Section 8 examines viscous energy transfer and dissipation in compressible flow, with particular attention to the second viscosity coefficient and Stokes' hypothesis. Finally, Section 9 collects the conclusions that the author draws from these examples and identifies the connection to the proposed asymmetric formulation developed in the subsequent study.

2. Fluid Stress Tensor and the Navier–Stokes Equations

This section introduces the general fluid stress tensor and the Navier–Stokes equations to establish the notation used throughout the investigation. The derivation is included so that the subsequent arguments can be related explicitly to the stress components and spatial derivatives appearing in the momentum balance.

2.1. Fluid Stress Tensor

2.1.1. General Fluid Stress Tensor

For a three-dimensional flow, the total stress tensor $\vec{\vec{T}}$ can be expressed in the following general form:

$$\vec{\vec{T}} = \begin{bmatrix} -p & 0 & 0 \\ 0 & -p & 0 \\ 0 & 0 & -p \end{bmatrix} + \begin{bmatrix} \tau_{11} & \tau_{12} & \tau_{13} \\ \tau_{21} & \tau_{22} & \tau_{23} \\ \tau_{31} & \tau_{32} & \tau_{33} \end{bmatrix} + \begin{bmatrix} \lambda \nabla \cdot \vec{V} & 0 & 0 \\ 0 & \lambda \nabla \cdot \vec{V} & 0 \\ 0 & 0 & \lambda \nabla \cdot \vec{V} \end{bmatrix} \tag{1}$$

Here the double arrow in $\vec{\vec{T}}$ denotes a second-order tensor, and p denotes the fluid pressure. Following the notation used in [9], the viscous contribution is written in a more explicit form as

$$\vec{\vec{\sigma}} = \begin{bmatrix} \tau_{11} & \tau_{12} & \tau_{13} \\ \tau_{21} & \tau_{22} & \tau_{23} \\ \tau_{31} & \tau_{32} & \tau_{33} \end{bmatrix} + \begin{bmatrix} \lambda \nabla \cdot \vec{V} & 0 & 0 \\ 0 & \lambda \nabla \cdot \vec{V} & 0 \\ 0 & 0 & \lambda \nabla \cdot \vec{V} \end{bmatrix}. \tag{2}$$

The first tensor on the right-hand side of Eq. (2) contains the viscous stress components, while the second term represents the contribution associated with volumetric deformation. The parameter λ is the second viscosity coefficient; the relation $\lambda = -\frac{2}{3}\mu$ is Stokes' hypothesis. Here τ_{ij} denotes a component of the viscous stress tensor, whose detailed expression depends on the constitutive formulation adopted in the analysis. The indices

$i, j = 1, 2, 3$ refer to the Cartesian directions x, y, z, respectively. The velocity vector may be written either as $\vec{V} = u_1\vec{i} + u_2\vec{j} + u_3\vec{k}$ or as $\vec{V} = u\vec{i} + v\vec{j} + w\vec{k}$. Thus (u_1, u_2, u_3) and (u, v, w) are alternative notations for the same three velocity components, and $\vec{i}, \vec{j}, \vec{k}$ are the corresponding unit vectors along the three coordinate axes. Both notations are retained below where they make the component expressions easier to follow.

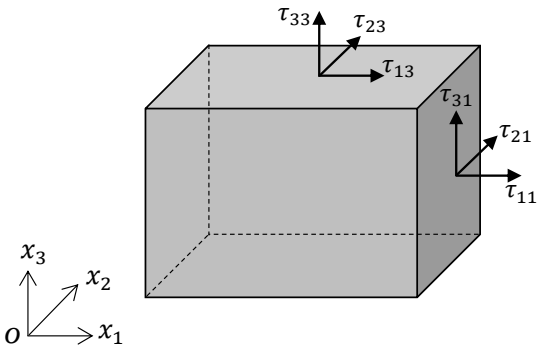


Figure 2. Viscous stress components on two faces of a fluid element.

The stress indices follow the convention used in [40]: the first index identifies the direction of the force component, and the second identifies the normal direction of the plane on which that component acts. For example, τ_{13} acts in the x direction on a plane of constant z. A first index of 2 or 3 therefore identifies a force component along the y or z direction, respectively. Similarly, a second index of 1 or 2 identifies a plane of constant x or y. Under this convention, τ_{31} acts in the z direction on a plane of constant x, whereas τ_{11} acts in the x direction on that same type of plane. The distinction between the force direction and the plane normal is essential when interpreting the components shown in Figure 2, particularly when a pair of complementary shear stresses is discussed.

2.1.2. General Fluid Stress Tensor: Viscous Force

Several approaches may be used to derive the momentum equations for fluid motion. These include the differential fluid-element method, which gives a direct representation of the forces acting on a small volume [9,41–43], and integral approaches based on the Reynolds transport theorem [11,40]. In each case, the viscous contribution must be expressed as the resultant of the stresses acting over the boundary of the selected volume. Following the differential approach associated with the classical derivations, the present discussion uses a small fluid element to display these contributions explicitly. This method is particularly useful here because the later arguments concern the interpretation of stress increments between neighbouring faces of that element.

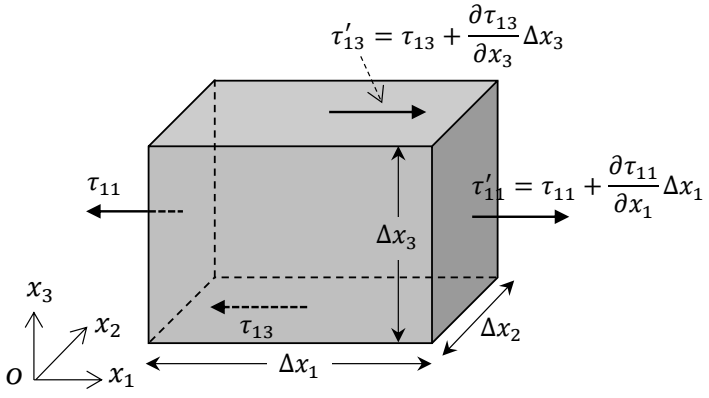


Figure 3. Fluid element used to derive the momentum equation.

The force calculation is illustrated by the selected stress components on the top, bottom, left, and right faces in Figure 3. The fluid element has dimensions $(\Delta x_1, \Delta x_2, \Delta x_3) = (\Delta x, \Delta y, \Delta z)$. These increments are taken to be sufficiently small for the first-order spatial expansions used in differential calculus. For example, the shear stress on the top face is written as $\tau'_{13} = \tau_{13} + \frac{\partial \tau_{13}}{\partial x_3}\Delta x_3$, relative to τ_{13} on the bottom face. Similarly, the normal-stress component on the right face is $\tau'_{11} = \tau_{11} + \frac{\partial \tau_{11}}{\partial x_1}\Delta x_1$, relative to τ_{11} on the left face. The prime therefore distinguishes the value evaluated after the stated spatial displacement; it does not denote a different constitutive coefficient. This notation follows the differential-element derivations presented in standard textbooks [8–14].

Using the difference between the normal stresses on the left and right faces, the net viscous force in the x direction due to τ_{11} and τ'_{11} is calculated as

$$\Delta F_{11} = \left(\tau_{11} + \frac{\partial \tau_{11}}{\partial x_1}\Delta x_1 - \tau_{11}\right)\Delta x_2 \Delta x_3 = \frac{\partial \tau_{11}}{\partial x_1}\Delta V, \tag{3}$$

Here $\Delta V = \Delta x_1 \Delta x_2 \Delta x_3$ is the element volume. Similarly, the force in the x direction arising from the shear components τ'_{12} and τ_{12} is

$$\Delta F_{12} = \left(\tau_{12} + \frac{\partial \tau_{12}}{\partial x_2}\Delta x_2 - \tau_{12}\right)\Delta x_1 \Delta x_3 = \frac{\partial \tau_{12}}{\partial x_2}\Delta V, \tag{4}$$

The corresponding force contribution from the shear components τ'_{13} and τ_{13} is

$$\Delta F_{13} = \left(\tau_{13} + \frac{\partial \tau_{13}}{\partial x_3}\Delta x_3 - \tau_{13}\right)\Delta x_1 \Delta x_2 = \frac{\partial \tau_{13}}{\partial x_3}\Delta V. \tag{5}$$

Adding these contributions gives the total viscous force on the element in the x direction:

$$\Delta F_1 = \Delta F_{11} + \Delta F_{12} + \Delta F_{13} = \left(\frac{\partial \tau_{11}}{\partial x_1} + \frac{\partial \tau_{12}}{\partial x_2} + \frac{\partial \tau_{13}}{\partial x_3}\right)\Delta V, \tag{6}$$

Dividing by the element volume gives the viscous force per unit volume in the x direction:

$$f_1^{vis} = \frac{\Delta F_1}{\Delta V} = \frac{\partial \tau_{11}}{\partial x_1} + \frac{\partial \tau_{12}}{\partial x_2} + \frac{\partial \tau_{13}}{\partial x_3}. \tag{7}$$

The corresponding viscous-force components per unit volume in the y and z directions are obtained by the same procedure:

$$f_2^{vis} = \frac{\partial \tau_{21}}{\partial x_1} + \frac{\partial \tau_{22}}{\partial x_2} + \frac{\partial \tau_{23}}{\partial x_3}, \tag{8}$$

$$f_3^{vis} = \frac{\partial \tau_{31}}{\partial x_1} + \frac{\partial \tau_{32}}{\partial x_2} + \frac{\partial \tau_{33}}{\partial x_3}. \tag{9}$$

At this stage of the derivation, no detailed constitutive expression has been assigned to the viscous stress components. In particular, their symmetry has not yet been imposed. The force expressions therefore identify the stress derivatives required by the momentum balance before a specific stress–velocity relation is introduced.

2.1.3. General Fluid Stress Tensor: Momentum Equations

Combining these viscous-force contributions with the pressure and body forces gives the following momentum equations for compressible flow. Detailed derivations are available in [9,41–43].

$$\begin{cases} \rho\left(\frac{\partial u_1}{\partial t}+u_1\frac{\partial u_1}{\partial x_1}+u_2\frac{\partial u_1}{\partial x_2}+u_3\frac{\partial u_1}{\partial x_3}\right)=-\frac{\partial p}{\partial x_1}+f_{b1}+\left(\frac{\partial \tau_{11}}{\partial x_1}+\frac{\partial \tau_{12}}{\partial x_2}+\frac{\partial \tau_{13}}{\partial x_3}\right)+\frac{\partial(\lambda\nabla\cdot\vec{V})}{\partial x_1}, \\ \rho\left(\frac{\partial u_2}{\partial t}+u_1\frac{\partial u_2}{\partial x_1}+u_2\frac{\partial u_2}{\partial x_2}+u_3\frac{\partial u_2}{\partial x_3}\right)=-\frac{\partial p}{\partial x_2}+f_{b2}+\left(\frac{\partial \tau_{21}}{\partial x_1}+\frac{\partial \tau_{22}}{\partial x_2}+\frac{\partial \tau_{23}}{\partial x_3}\right)+\frac{\partial(\lambda\nabla\cdot\vec{V})}{\partial x_2}, \\ \rho\left(\frac{\partial u_3}{\partial t}+u_1\frac{\partial u_3}{\partial x_1}+u_2\frac{\partial u_3}{\partial x_2}+u_3\frac{\partial u_3}{\partial x_3}\right)=-\frac{\partial p}{\partial x_3}+f_{b3}+\left(\frac{\partial \tau_{31}}{\partial x_1}+\frac{\partial \tau_{32}}{\partial x_2}+\frac{\partial \tau_{33}}{\partial x_3}\right)+\frac{\partial(\lambda\nabla\cdot\vec{V})}{\partial x_3}, \end{cases} \tag{10}$$

Here ρ is the fluid density, and f_{b1}, f_{b2}, f_{b3} are the body-force components per unit volume in the x, y, and z directions. Gravity is a common example of such a force and acts vertically downwards. With the Cartesian coordinates shown in Figure 3, its components are $f_{b1} = f_{b2} = 0$ and $f_{b3} = -\rho g$. The negative sign indicates that the gravitational force acts opposite to the positive z direction. Defining the body force per unit volume in this way keeps its units consistent with the stress-gradient terms in the momentum equations.

Using the Einstein summation convention, the momentum equation can be written more compactly as

$$\rho\left(\frac{\partial u_i}{\partial t}+u_j\frac{\partial u_i}{\partial x_j}\right)=-\frac{\partial p}{\partial x_i}+f_{bi}+\frac{\partial \tau_{ij}}{\partial x_j}+\frac{\partial}{\partial x_i}\left(\lambda\frac{\partial u_k}{\partial x_k}\right). \tag{11}$$

Here $\frac{\partial u_k}{\partial x_k}=\frac{\partial u_1}{\partial x_1}+\frac{\partial u_2}{\partial x_2}+\frac{\partial u_3}{\partial x_3}$.

2.2. Symmetric Stress Tensor (SST) for Fluids

2.2.1. Symmetric Stress Tensor for Fluids: Why Is It Required?

The conventional stress tensor is symmetric under the assumptions of classical continuum mechanics without applied body couples or independent internal angular momentum. Historical discussions connect this condition with Cauchy's treatment of moment balance [6]. For completeness, the familiar small-element argument is outlined below, using a solid element to introduce the relevant stress pairs. The same general balance principle is commonly adopted in the classical treatment of fluids. The present author questions aspects of its interpretation when applied to the fluid examples examined in Sections 5–7. Those sections develop the author's proposed objections, while the subsequent study [17] considers an asymmetric formulation intended to address them. The distinction between the conventional balance requirement and the additional assumptions made in the present argument should therefore remain explicit throughout the comparison.

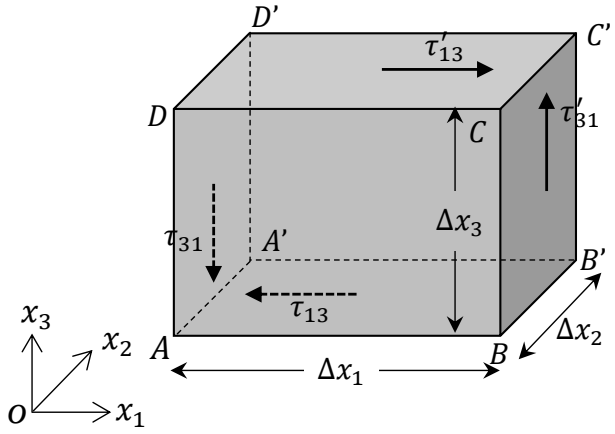


Figure 4. Element and reference axes used in the stress-symmetry argument.

Consider the solid element in Figure 4. Following the moment-balance construction discussed in [12,16], choose AA' as the reference axis. In the diagram, τ'_{31} on the right

vertical face produces an anticlockwise moment, while τ'_{13} on the top face produces a clockwise moment. Taking anticlockwise moments as positive and clockwise moments as negative, the respective contributions about the selected axis are written as

$$\begin{cases} \Delta M_1 = (\tau'_{31}\Delta x_2\Delta x_3)\Delta x_1 = \tau'_{31}\Delta V \quad \text{(anticlockwise)}, \\ \Delta M_2 = -(\tau'_{13}\Delta x_1\Delta x_2)\Delta x_3 = -\tau'_{13}\Delta V \quad \text{(clockwise)}. \end{cases} \tag{12}$$

The resultant moment about the selected axis AA' is therefore

$$\Delta M = \Delta M_1 + \Delta M_2 = (\tau'_{31} - \tau'_{13})\Delta V. \tag{13}$$

Following the infinitesimal-element argument in [12], the condition used to exclude an unbounded angular acceleration is

$$\tau'_{13} = \tau'_{31}. \tag{14}$$

Choosing CC' as the reference axis gives the corresponding relation for the stresses on the bottom and left faces. Under the same construction, the complementary pair must satisfy $\tau_{31} = \tau_{13}$. The pair selected therefore changes with the reference axis used in the element diagram.

Repeating the moment comparison for the remaining complementary stress pairs gives

$$\tau_{12} = \tau_{21};\ \tau_{23} = \tau_{32}. \tag{15}$$

This construction gives a symmetric stress tensor for a classical solid element when the assumptions exclude additional applied couples or internal moments. It is associated with the balance of angular momentum, and Cauchy's extension of stress concepts to fluid motion is discussed in [6]. The same symmetry condition is widely used in standard fluid-mechanics treatments [8–14,40]. The present investigation asks whether the interpretation of this condition requires further examination when the material deforms continuously as a fluid. In the author's argument, the examples considered below reveal difficulties in constructing viscous-force increments and in applying differential calculus to planar Poiseuille flow. These proposed difficulties are examined through the stated element constructions and should be read as the conclusions of that argument rather than as assumptions already established by the preceding moment balance.

2.2.2. Constructing the Symmetric Stress Tensor for Fluids

Textbooks construct the viscous stress tensor through several complementary presentations, including physical reasoning [9,40,44], graphical descriptions of element deformation [12,14,42], and a mathematical formulation of the constitutive relation [11]. Although the notation and sequence of the derivations differ, these approaches produce the same conventional component expressions for an isotropic Newtonian fluid, such as air or water under the applicable conditions. The following expression is the common starting point for the comparisons made in this section:

$$\left.\begin{aligned} \tau_{11} = 2\mu\left(\frac{\partial u_1}{\partial x_1}\right);\ \tau_{22} = 2\mu\left(\frac{\partial u_2}{\partial x_2}\right);\ \tau_{33} = 2\mu\left(\frac{\partial u_3}{\partial x_3}\right) \\ \tau_{12} = \tau_{21} = \mu\left(\frac{\partial u_1}{\partial x_2} + \frac{\partial u_2}{\partial x_1}\right) \\ \tau_{13} = \tau_{31} = \mu\left(\frac{\partial u_1}{\partial x_3} + \frac{\partial u_3}{\partial x_1}\right) \\ \tau_{23} = \tau_{32} = \mu\left(\frac{\partial u_3}{\partial x_2} + \frac{\partial u_2}{\partial x_3}\right) \end{aligned}\right\} \tag{16}$$

2.2.2.1 Graphical Transformation of a Fluid Element

Following Houghton et al. [42], with related presentations in [12,14], the motion of a small fluid element is separated into shear deformation and rotation, as illustrated in Figure 5. The angular changes α and β describe the displacement of the initially perpendicular sides. In this representation, $\frac{1}{2}(\alpha - \beta)$ describes rotation, while $\frac{1}{2}(\alpha + \beta)$ describes the tensorial shear deformation. The angles used in this construction are expressed in terms of the local velocity gradients as follows:

$$\alpha = \frac{\partial v}{\partial x}\Delta t \quad \text{and} \quad \beta = \frac{\partial u}{\partial y}\Delta t, \tag{17}$$

The rate of shear strain in the $x - y$ plane is given by

$$\dot{\gamma}_{xy} = \frac{d}{dt}\left(\frac{\alpha + \beta}{2}\right) = \frac{1}{2}\left(\frac{\partial u}{\partial y} + \frac{\partial v}{\partial x}\right). \tag{18}$$

The notation in Eq. (18) requires care: if the angles in Eq. (17) represent changes during a finite time interval, they should be denoted by $\Delta\alpha$ and $\Delta\beta$. This distinction separates an angular increment from its rate of change. The presentation otherwise follows the approach used in the cited textbooks [42,43,45,46].

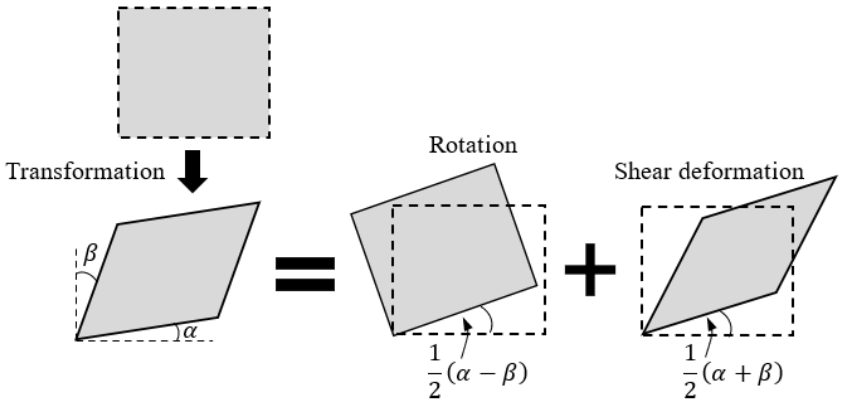


Figure 5. Deformation and rotation of a fluid element.

The corresponding rotation of the element is calculated as

$$\omega = \frac{d}{dt}\left(\frac{\alpha - \beta}{2}\right) = \frac{1}{2}\left(\frac{\partial u}{\partial y} - \frac{\partial v}{\partial x}\right). \tag{19}$$

The same decomposition can also be displayed directly through a mathematical rearrangement of the velocity gradient appearing in Newton's law of viscosity. Writing the gradient as the sum of symmetric and antisymmetric contributions gives the following expression:

$$\frac{\partial u}{\partial y} = \frac{1}{2}\left(\frac{\partial u}{\partial y} + \frac{\partial v}{\partial x}\right) + \frac{1}{2}\left(\frac{\partial u}{\partial y} - \frac{\partial v}{\partial x}\right). \tag{20}$$

The velocity gradient $\frac{\partial u}{\partial y}$ is thus written as the sum of a symmetric contribution and an antisymmetric contribution. These terms are associated, respectively, with the deformation and local rotation of the fluid element. Their sum recovers the original gradient, so the decomposition can be checked directly without changing the underlying velocity field.

To recover the conventional stress expression in Eq. (16) from the tensorial shear rate in Eq. (18), a factor of two is introduced. This ensures that μ has the meaning of dynamic viscosity used in Newton's law, illustrated in Figure 1. The explanation in [42] connects this factor with the one-half appearing in the definition of the tensorial shear-strain rate. The author questions whether that explanation, when expressed only as a matter of

mathematical convenience, adequately communicates the physical basis of the constitutive coefficient.

The author's concern is that a numerical coefficient in a physical relation should be explained through the definition and physical meaning of the quantities involved. Merely describing a coefficient as convenient can obscure the distinction between different conventions. For comparison, the expressions $\frac{1}{2}mv^2$ and mv^2 differ only by a factor of two, but they cannot both represent the kinetic energy of the same mass m moving at velocity v under the same definition. The first is the familiar kinetic-energy expression, whereas the second is twice that energy. This example illustrates the author's request for a clear explanation of the convention used in constructing the shear-strain rate and the associated viscous stress.

Other presentations, including those of Anderson [47], Hibbeler [13], and Le Méhauté [14], express the shear rate without the one-half used in the tensorial definition. In that notation, the corresponding expression is written as

$$\dot{\gamma}_{xy} = \frac{\partial u}{\partial y} + \frac{\partial v}{\partial x}. \tag{21}$$

The two expressions therefore differ in the convention used to define shear rate. The author considers this distinction important because an unexplained change of convention can make the constitutive coefficient appear arbitrary. For the comparison developed here, Eq. (21) is read together with the stress relation to which it is applied, so that the coefficient and the definition of shear rate can be examined as a pair.

The Author's Argument.

The author's position is that the velocity gradient and the associated viscous stress should be introduced together when explaining Newton's law of viscosity, as in Figure 1. In a steady flow, both quantities are present simultaneously, even though the velocity at a fixed spatial location does not vary with time. Explaining the stress through this spatial variation may help distinguish the rate of material deformation from the time derivative of a field variable measured at a fixed point. Without that distinction, a reference to a "time rate" in a steady flow can make the physical interpretation less clear than the underlying relation requires.

The kinematic construction of the symmetric rate-of-strain tensor does not, by itself, specify the material. It can therefore be used to describe deformation in both Newtonian and non-Newtonian fluids. The author's question concerns the subsequent constitutive step: how should symmetry of the resulting stress be established when the relation between stress and deformation rate is nonlinear or direction dependent? To illustrate the concern, suppose that the gradient $\frac{\partial u}{\partial y}$ is associated with a contribution $\mu_1 \frac{\partial u}{\partial y}$, while the gradient $\frac{\partial v}{\partial x}$ is associated with $\mu_2 \frac{\partial v}{\partial x}$. The proposed combined expression is then $\tau_{xy} = \mu_1 \frac{\partial u}{\partial y} + \mu_2 \frac{\partial v}{\partial x} = \tau_{yx}$. In the author's interpretation, identifying both terms with a single Newtonian viscosity requires $\mu_1 = \mu_2 = \mu$. The example is intended to distinguish the purely kinematic definition from the material relation that converts deformation rate into stress. The author raises a similar question for a fluid whose properties vary with position or direction. These cases should be distinguished carefully: spatial variation, directional dependence, and nonlinear response are different constitutive issues, even though each may complicate the interpretation of a simple componentwise viscosity relation. The argument here asks for those material assumptions to be stated explicitly before the stress components are compared.

2.2.2.2 The Physical Reasoning Method

Following Newman [40], the conventional viscous stress tensor can be introduced by considering the properties that a Newtonian constitutive relation should possess in a general velocity field. Two requirements are particularly relevant to the present discussion:

1) Each viscous stress component is taken to depend linearly on the nine velocity gradients $\frac{\partial u_i}{\partial x_j}$. Under this assumption, a spatially uniform translational velocity produces no

viscous stress because every velocity gradient vanishes. This is termed the first requirement in the discussion below.

2) The shear contribution is constructed from the symmetric combination $\frac{\partial u_i}{\partial x_j} + \frac{\partial u_j}{\partial x_i}$. For rigid-body rotation, this combination vanishes, giving zero viscous stress and zero viscous dissipation under the conventional Newtonian relation. This is termed the second requirement in the subsequent argument.

The second requirement leads to a symmetric viscous stress tensor in the conventional construction. The author nevertheless asks whether these requirements alone adequately explain the coefficients used in the complete component expression, Eq. (16). The numerical factors must be interpreted together with the adopted definition of deformation rate, as discussed above. A further question concerns the physical meaning of zero stress during rigid rotation when an external load requires torque transmission. The examples in Section 7 are used to develop that question by comparing an unloaded rotating state with a proposed arrangement involving a loaded inner shaft.

2.2.2.3 The Mathematical Constitutive Relation

Kundu et al. [11] develop the constitutive relation through a tensor formulation and the relevant transformation and material-symmetry requirements. The symmetric part of the velocity gradient is denoted by $S_{ij} = \frac{1}{2}(\frac{\partial u_i}{\partial x_j} + \frac{\partial u_j}{\partial x_i})$. It describes the rate of deformation used in the conventional Newtonian stress relation. To express a general linear dependence on this tensor, the constitutive coefficients are first collected into a fourth-order tensor. The resulting relation is written in the following form:

$$\tau_{ij} = K_{ijmn} S_{mn}. \tag{22}$$

The author finds this fourth-order tensor representation less immediately transparent than the componentwise descriptions introduced above. The tensor K_{ijmn} has 81 components before the relevant material symmetries and other restrictions are imposed, and its role is to map the rate-of-strain tensor to the viscous stress tensor. The concern raised here is therefore about the physical assumptions underlying the reduction of those components, rather than the notation alone. Following the constitutive construction described in [11], the relation is reduced to the form

$$\tau_{ij} = 2\mu S_{ij} + \lambda S_{mm} \delta_{ij}, \tag{23}$$

This reduced expression provides the conventional symmetric viscous stress tensor. The author nevertheless asks whether the assumptions required to pass from Eq. (22) to Eq. (23) are sufficiently explicit for the practical examples examined here. An algebraically consistent reduction does not, by itself, identify the range of physical conditions under which the resulting constitutive relation should be applied. Particular attention is therefore directed to the final term and the interpretation of the coefficient associated with compressibility. Discussions of the second viscosity coefficient in [48,49] provide relevant context for this question. The later section on energy dissipation returns to that coefficient and to the additional restriction introduced by Stokes' hypothesis.

2.2.3. Symmetric Stress Tensor in the Navier–Stokes Equations

Substitution of the Newtonian SST in Eq. (16) into the x-direction viscous-force expression, Eq. (8), gives

$$f_1^{vis} = \mu\left(\frac{\partial^2 u_1}{\partial x_1 \partial x_1} + \frac{\partial^2 u_1}{\partial x_2 \partial x_2} + \frac{\partial^2 u_1}{\partial x_3 \partial x_3}\right) + \mu \frac{\partial}{\partial x_1}\left(\frac{\partial u_1}{\partial x_1} + \frac{\partial u_2}{\partial x_2} + \frac{\partial u_3}{\partial x_3}\right), \tag{24}$$

In the Einstein summation convention, the same component is written as

$$f_1^{vis} = \mu \frac{\partial^2 u_1}{\partial x_j \partial x_j} + \mu \frac{\partial}{\partial x_1}\left(\frac{\partial u_k}{\partial x_k}\right). \tag{25}$$

The other two components of the viscous force are obtained in the same manner:

$$\begin{cases} f_2^{vis} = \mu \dfrac{\partial^2 u_2}{\partial x_j \partial x_j} + \mu \dfrac{\partial}{\partial x_2}\left(\dfrac{\partial u_k}{\partial x_k}\right), \\ f_3^{vis} = \mu \dfrac{\partial^2 u_3}{\partial x_j \partial x_j} + \mu \dfrac{\partial}{\partial x_3}\left(\dfrac{\partial u_k}{\partial x_k}\right). \end{cases} \tag{26}$$

The resulting Navier–Stokes momentum equation therefore takes the form

$$\rho\left(\frac{\partial u_i}{\partial t} + u_j \frac{\partial u_i}{\partial x_j}\right) = -\frac{\partial p}{\partial x_i} + f_{bi} + \mu \frac{\partial^2 u_i}{\partial x_j \partial x_j} + (\mu + \lambda)\frac{\partial}{\partial x_i}\left[\frac{\partial u_k}{\partial x_k}\right]. \tag{27}$$

Imposing Stokes' hypothesis, $\lambda = -\frac{2}{3}\mu$, gives the following expression:

$$\rho\left(\frac{\partial u_i}{\partial t} + u_j \frac{\partial u_i}{\partial x_j}\right) = -\frac{\partial p}{\partial x_i} + f_{bi} + \mu \frac{\partial^2 u_i}{\partial x_j \partial x_j} + \frac{1}{3}\mu \frac{\partial}{\partial x_i}\left[\frac{\partial u_k}{\partial x_k}\right]. \tag{28}$$

For incompressible motion, $\frac{\partial u_k}{\partial x_k} = 0$, and the momentum equation reduces to

$$\rho\left(\frac{\partial u_i}{\partial t} + u_j \frac{\partial u_i}{\partial x_j}\right) = -\frac{\partial p}{\partial x_i} + f_{bi} + \mu \frac{\partial^2 u_i}{\partial x_j \partial x_j}. \tag{29}$$

Both the general momentum balance in Eq. (11) and the incompressible form in Eq. (29) are familiar from standard textbooks. They are included here to establish a consistent reference for the later discussion. In particular, the distinction between a balance equation written in terms of unspecified stresses and a closed equation using a particular constitutive relation will be important in interpreting the subsequent arguments.

3. Symmetric Stress Tensor: How Is It Applied to Fluids?

The conventional SST appears in both derivations of the Navier–Stokes equations and practical calculations based on them. The present author nevertheless identifies a potential inconsistency between the interpretation of the tensor and the component expressions used in surface-force calculations. In Section 5, the issue is examined through stress increments on a fluid element. Here the focus is on the familiar expressions for lift and drag on an airfoil. The argument asks whether every stress contribution that the author associates with the symmetry condition has been included on the appropriate surface. The following example sets out that proposed discrepancy before applying a related construction to Stokes flow past a sphere.

The conventional surface-force construction is illustrated in Figure 6, with lift acting along the y axis and drag along the x axis. In local wall coordinates, the tangential shear stress is commonly written as

$$\tau = \mu\left(\frac{\partial u}{\partial y}\right)_{y=0}, \tag{30}$$

Here u is the velocity tangential to the wall, and y is the coordinate perpendicular to the local surface. This form of the wall-shear relation appears in the cited textbooks [9,11,12,40,42,47]. Its use depends on the local coordinate convention and the wall conditions assumed in the derivation.

The airfoil force is obtained by combining the local tangential wall shear stress τ with the pressure p, which acts normally to the surface. These quantities may be obtained from wind-tunnel measurements, flight measurements, or a numerical flow solution. Resolving their contributions along and perpendicular to the incoming flow gives the drag d and lift l, respectively. For the notation adopted here, the resulting expressions are written as in [9,47]:

$$\begin{cases} l = \int_{LE}^{TE} (-p_u \cos\theta + \tau_u \sin\theta)\, ds + \int_{LE}^{TE} (-p_l \cos\theta + \tau_l \sin\theta)\, ds, \\ d = \int_{LE}^{TE} (-p_u \sin\theta + \tau_u \cos\theta)\, ds + \int_{LE}^{TE} (-p_l \sin\theta + \tau_l \cos\theta)\, ds, \end{cases} \tag{31}$$

The integrations extend from the leading edge (LE) to the trailing edge (TE) on both airfoil surfaces. The subscripts u and l identify quantities on the upper and lower surfaces, respectively.

These surface-force expressions have been used extensively in practical aerodynamic calculations, and their successful application is central to conventional engineering practice. Discussions of CFD in aircraft design include the Airbus A380 [50] and Boeing 787 [51], illustrating the importance of such calculations in advanced aerospace applications. The author previously accepted the expressions without questioning their consistency with the interpretation of the stress tensor considered here. The issue now raised is more specific: whether the complementary component implied by stress symmetry has been assigned to the appropriate surface when the local force contributions are assembled. The following discussion develops the author's interpretation of that question.

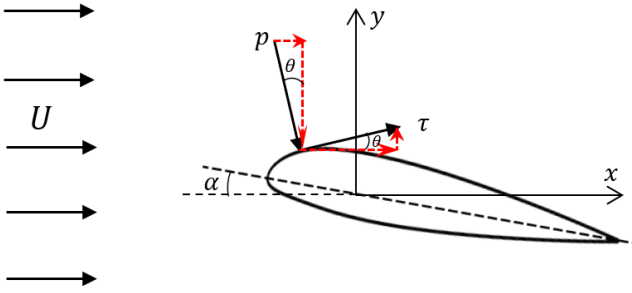


Figure 6. Pressure and wall shear on an airfoil at angle of attack α.

The Author's Argument.

The author's concern is that the conventional force calculation does not include a contribution that the author associates with the complementary stress component. In the proposed construction, this component is denoted by τ' and shown in red in Figure 7. It is assigned a direction perpendicular to the tangential wall shear stress τ defined in Eq. (30), with equal magnitude, $\tau' = \tau$. Under this interpretation, the additional component is normal to the local airfoil surface, as is the pressure contribution. The author regards its sign as requiring a separate directional convention and, for the illustration below, chooses it to act opposite to the pressure. The resulting formulas therefore follow from that explicit assignment of the additional component. This assignment is the premise being examined in the argument, rather than a change to the measured pressure or tangential wall shear.

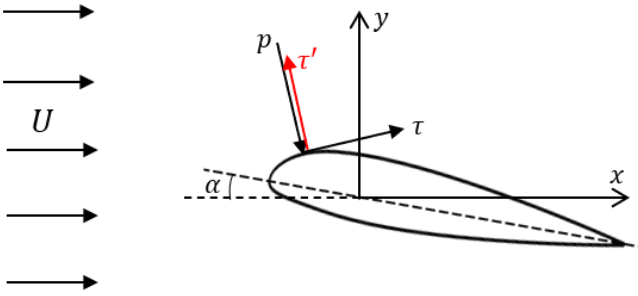


Figure 7. The additional airfoil stress contribution proposed in the author extquotesingle s interpretation.

With the additional contribution assigned as described above, the author applies Newton's third law to assemble the proposed surface forces. The resulting expressions for lift and drag are then written as follows:

$$\begin{cases} l = \int_{LE}^{TE} \left[(\tau_u' - p_u) \cos\theta + \tau_u \sin\theta \right] ds + \int_{LE}^{TE} \left[(\tau_l' - p_l) \cos\theta + \tau_l \sin\theta \right] ds, \\ d = \int_{LE}^{TE} \left[(\tau_u' - p_u) \sin\theta + \tau_u \cos\theta \right] ds + \int_{LE}^{TE} \left[(\tau_l' - p_l) \sin\theta + \tau_l \cos\theta \right] ds. \end{cases} \tag{32}$$

The author is not aware of these particular expressions being used in conventional lift and drag calculations. Within the proposed interpretation, however, they are regarded as necessary to include all the assigned surface-force contributions. Any additional normal viscous traction would also need to be included if it were nonzero under the relevant wall conditions, including cases involving a moving surface.

It might be argued that the added normal contribution would be small relative to pressure in many aerodynamic applications. Under that assumption, Eq. (31) could remain a close approximation to the proposed expression, particularly for attached flows. The magnitude of the discrepancy would then depend on the relative sizes of the pressure and the stress contribution introduced by the author's construction.

The author's position is that a complete force calculation must include every traction contribution actually assigned to the surface, regardless of whether the constitutive tensor is symmetric or asymmetric. In the proposed interpretation, this means combining the tangential stress, the additional normal contribution, and pressure before resolving lift and drag. Omitting a contribution regarded as physically present would leave the stated force balance incomplete. The issue is more conspicuous in the author's treatment of Stokes flow past a sphere, because the viscous and pressure contributions are comparable in the creeping-flow force balance. That example therefore offers a clearer comparison than a high-Reynolds-number airfoil configuration in which pressure may dominate. As shown in Section 6, the author's inclusion of the additional contribution leaves the calculated drag unchanged but produces a nonzero lift. The symmetry of the physical flow requires that this transverse resultant vanish. The resulting discrepancy is used to motivate the author's objection to the conventional interpretation, while making the assumed assignment of the additional stress contribution the central point for assessment.

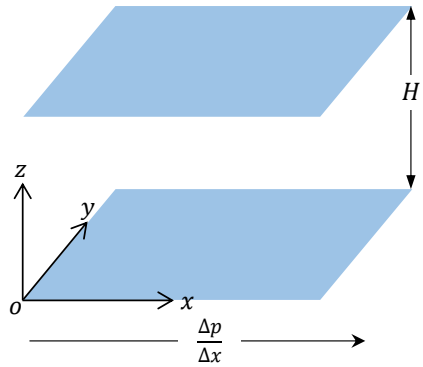


Figure 8. Parallel-plate configuration used to discuss planar Poiseuille flow.

4. Planar Poiseuille Flow: A Simple Example

Planar Poiseuille flow is a steady laminar flow between two stationary parallel plates of effectively infinite extent, as shown in Figure 8. The flow is driven by the imposed streamwise pressure gradient $\frac{\Delta p}{\Delta x}$. Its simple geometry permits an explicit velocity solution

and an equally explicit evaluation of the stress components. The following assumptions define the configuration considered here:

1. The pressure-driven velocity is directed along the x axis. Since the plates are stationary and the idealised configuration is uniform in their plane, the transverse velocity components are taken to be zero: $v = 0$ and $w = 0$.

2. The streamwise velocity depends only on the coordinate across the channel. It is therefore written as $u = u(z)$ and is independent of both the streamwise coordinate x and the spanwise coordinate y.

With these velocity assumptions, the vanishing terms are removed from the momentum equations, leaving

$$\begin{cases} 0 = -\dfrac{\partial p}{\partial x} + \mu \dfrac{\partial^2 u}{\partial z^2}, \\ 0 = -\dfrac{\partial p}{\partial y}, \\ 0 = -\dfrac{\partial p}{\partial z} - \rho g. \end{cases} \tag{33}$$

The second and third components of Eq. (33) give the following pressure distribution [52]:

$$p = -\rho g z + \left(\frac{\Delta p}{\Delta x}\right) x. \tag{34}$$

The pressure datum is chosen so that $p = 0$ at $x = 0$ and $z = 0$. Unlike presentations that omit gravity or absorb the hydrostatic contribution into a modified pressure, this expression retains the dependence on z. That dependence represents the hydrostatic pressure variation and does not introduce a separate velocity component in the vertical direction. The assumed flow therefore remains consistent with a streamwise velocity that varies only across the channel.

Solving the first component of Eq. (33) and imposing the no-slip conditions $u|_{z=H} = 0$ and $u|_{z=0} = 0$ gives the streamwise velocity distribution

$$u = -\frac{1}{2\mu}\left(\frac{\Delta p}{\Delta x}\right)(H - z)z. \tag{35}$$

The resulting parabolic velocity distribution is illustrated in Figure 9, showing the zero velocities at the stationary plates.

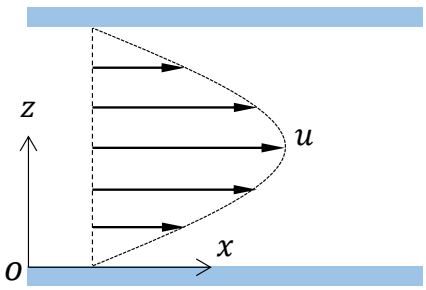


Figure 9. Planar Poiseuille velocity distribution under the imposed pressure gradient $\Delta p/\Delta x$.

Substituting this velocity distribution into the SST gives the following stress components:

$$\tau_{xz} = \tau_{zx} = \mu\left(\frac{\partial u}{\partial z} + \frac{\partial w}{\partial x}\right) = \left(\frac{\Delta p}{\Delta x}\right)\left(z - \frac{1}{2}H\right). \tag{36}$$

The complementary shear components are equal and are generally nonzero away from the channel centreline. Their directions on the selected element faces are illustrated

in Figure 10. This diagram provides the basis for the author's comparison between stress directions and the components of the velocity field.

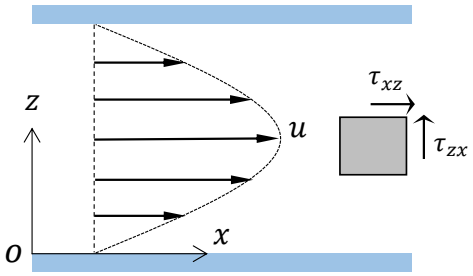


Figure 10. Velocity distribution and viscous stress components in planar Poiseuille flow.

The component τ_{xz} acts in the direction of the horizontal velocity, which the author regards as directly consistent with the usual description of viscous resistance. Equation (36) also gives a nonzero complementary component τ_{zx}, although the planar Poiseuille velocity field has no vertical component. The author interprets this as a difficulty in relating the tensor components to the statement that a fluid deforms continuously under shear. This interpretation motivates the subsequent discussion of the two stress components and their spatial increments, rather than introducing a different velocity solution for the same channel flow.

The next section examines the spatial increments of these stresses in more detail. The author uses the planar Poiseuille solution to argue that the selected finite-element symmetry construction cannot be maintained when the corresponding directional derivatives are applied. The argument therefore concerns the interpretation of the stress-pair construction in conjunction with differential calculus.

5. Proposed Conflicts Associated with the Symmetric Fluid Stress Tensor

The author's earlier study [15] identified what it interpreted as an inconsistency between the SST and the definition of a fluid, particularly in simple shear flow. The preceding section extends that concern to planar Poiseuille flow. To examine the argument more closely, the following subsections make the selected element geometry, stress pairs, and directional increments explicit. The purpose is to expose the intermediate steps on which the proposed objections depend, so that the relationship between the assumed symmetry condition and the resulting conclusions can be assessed.

Four proposed consequences are considered in this section: spatially uniform viscous stresses across the fluid domain; the resulting inability to construct the viscous-force term in the Navier–Stokes equations; direct dependence of the stress comparison on the element aspect ratio; and an apparent conflict with differential calculus in planar Poiseuille flow. Each consequence follows from the author's selected stress-pair interpretation. Further examples involving a sphere, rotating fluids, and compressible deformation are examined in Sections 6–8.

5.1. The Proposed Uniform-Stress Field

To isolate the proposed issue, Figure 11(a) shows only the shear components τ'_{13}, τ'_{31}, τ_{13}, and τ_{31} on the top, bottom, left, and right faces. No particular velocity distribution is specified at this stage. Following the construction in Section 2.2 and the related moment-balance discussions in [12,16], take AA' as the reference axis. In the diagram, the lines of action of τ_{13} and τ_{31} pass through that axis, whereas the two primed components produce moments of opposite sign. The author's application of the symmetry condition then gives $\tau'_{13} = \tau'_{31}$. With the element dimensions included in the respective force and moment-arm factors, the two contributions are taken to cancel about the selected axis. The argument uses this stress-pair construction as its starting point; the conventional treatment of stress symmetry and moment balance is discussed in the textbooks cited here [11,40].

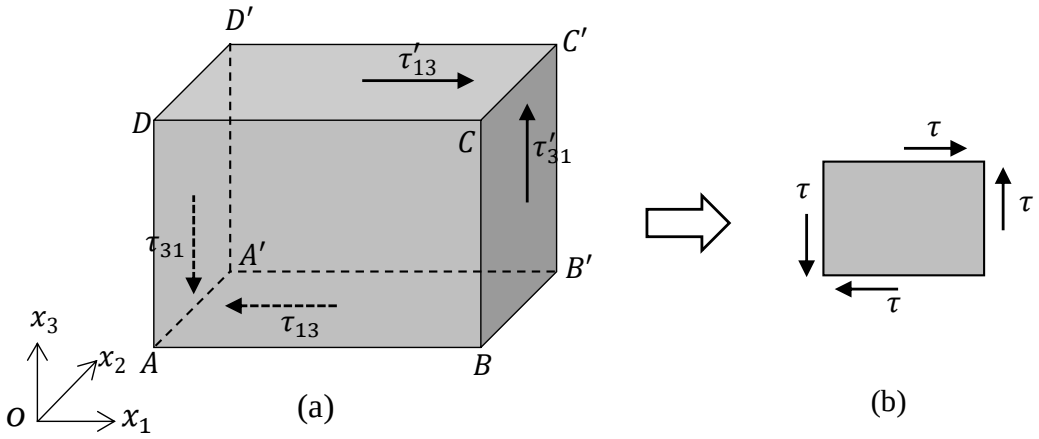


Figure 11. Proposed shear-stress construction: (a) complementary pairs; (b) equal face magnitudes.

Selecting CC' as the reference axis similarly gives the second pair, $\tau_{13} = \tau_{31}$. These complementary pairs are commonly illustrated by an element diagram of the type shown in Figure 11(a). The author's next step is to repeat the construction using the remaining corners as reference axes, rather than ending the comparison with the two pairs already identified.

Using DD' as the reference axis, the author obtains the proposed relation $\tau'_{31} = \tau_{13}$. Repeating the argument about BB' gives $\tau'_{13} = \tau_{31}$. These additional relations connect primed and unprimed components on different faces and are therefore the essential step in the uniform-stress argument developed below.

Combining the four proposed pairwise equalities gives $\tau_{13} = \tau_{31} = \tau'_{13} = \tau'_{31} = \tau$, as illustrated in Figure 11(b). A related element drawing appears in [45]. The author interprets the combined relations as requiring every displayed shear component on the selected element to have the same magnitude. Under this construction, the element therefore has no difference between the shear-stress magnitudes assigned to opposite faces. The subsequent extension to neighbouring elements depends on carrying this finite-element equality across their shared boundaries.

The author then extends the element argument to a collection of neighbouring fluid elements as follows.

Consider four neighbouring elements, E^1, E^2, E^3, and E^4, within the fluid domain. They are drawn separately in Figure 12 to make their boundary stresses visible, although their corresponding faces are understood to coincide in the actual construction. The right face of E^1 is shared with the left face of E^2, and the top face of E^1 is shared with the bottom face of E^3. The remaining interfaces are interpreted in the same way. The argument therefore compares stresses across shared boundaries rather than treating the illustrated gaps as physical spaces.

Newton's third law requires equal and opposite tractions on the two sides of each shared interface.

Assign the magnitude τ to the shear components of E^1, following the construction in Figure 11(b). The opposing tractions on its shared boundaries then have the same magnitude in E^2 and E^3. Their directions are reversed across each interface, as required by the action–reaction relation used in the argument.

Applying the same element construction to E^2 and E^3, the author assigns the magnitude τ to their remaining shear components. Repetition gives the same assignment for E^4, as illustrated in Figure 12. Extending this procedure throughout a connected domain leads the author to infer a spatially uniform shear-stress magnitude, irrespective of the specified flow conditions. This inference depends on the combined face-to-face equalities introduced above and is the basis of the proposed contradiction with nonuniform viscous flow.

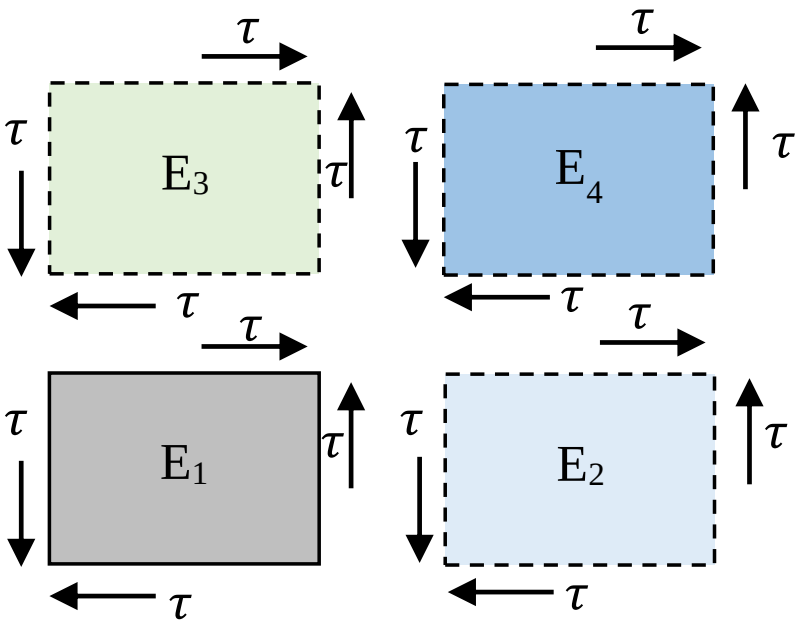


Figure 12. Neighbouring elements E^1–E^4, drawn separately to display the shared-face stresses.

A related question is whether the same element argument would imply spatially uniform stresses in a solid. The author considers this possible in the absence of the additional internal force and moment variations associated with deformation. A cantilever carrying a concentrated load at its free end provides a familiar comparison: the internal shear force is constant along the unloaded span [53]. The cross-sectional stress distribution and its relation to that resultant must nevertheless be distinguished when the example is used to interpret the stresses on an individual material element.

The author distinguishes this proposed fluid result from the internal-force distribution in a deforming solid. In a solid, structural deformation is associated with internal forces and moments whose distributions depend on the loading and geometry. In a classical fluid model, pressure and viscous stress provide the internal contact-force description, unless additional physical effects introduce further force or couple terms. Examples involving an electric field acting on polarised fluid molecules are discussed in [11]. The author's argument assumes that the usual symmetry requirement remains applicable in the absence of such additional effects. When that requirement is interpreted through the preceding face-to-face equalities, the author concludes that no shear-stress increments can arise. The proposed absence of a viscous resultant therefore follows from the uniformity inference, not from an independently specified velocity solution.

5.2. The Proposed Objection to Deriving the Navier–Stokes Equations

The differential fluid-element method is widely used to derive the Navier–Stokes equations because it displays the local force balance directly [9,41–43]. In Figure 13, the element dimensions are Δx_1, Δx_2, and Δx_3 along the x, y, and z directions. Small differences between stresses on opposing faces provide the viscous-force contribution. The comparison below examines those spatial differences in relation to the author's uniform-stress inference.

In the standard differential construction, the stress on the top face is expanded as $\tau'_{13} = \tau_{13} + \frac{\partial \tau_{13}}{\partial x_3}\Delta x_3$ relative to the value on the bottom face. Likewise, the stress on the right face is expanded as $\tau'_{31} = \tau_{31} + \frac{\partial \tau_{31}}{\partial x_1}\Delta x_1$ relative to the value on the left face. These expressions associate each change with a specified direction of displacement, as shown in Figure 13. Their differences, multiplied by the appropriate face areas, generate the force contributions used in the momentum equation. The derivation in Section 2 follows this

procedure. The author now compares it with the equality of opposite-face magnitudes inferred from the earlier element construction.

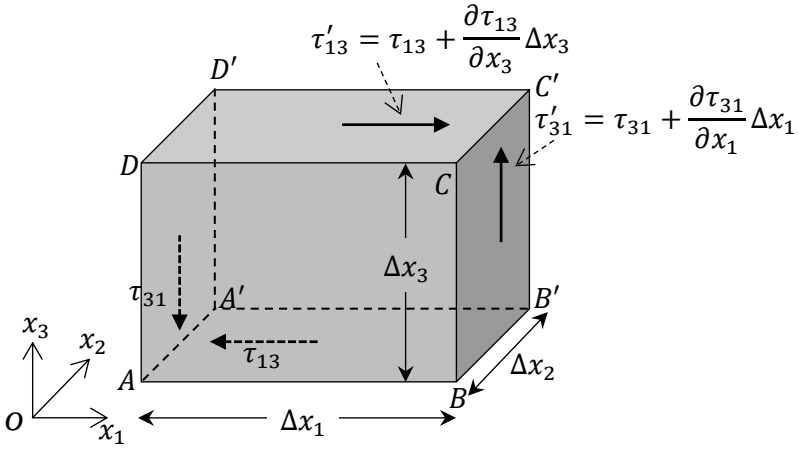


Figure 13. Fluid element and stress increments used in the momentum-equation derivation.

Under the author's interpretation of Figures 11(b) and 12, the symmetry requirement eliminates the stress increments just described. A uniform stress magnitude on the selected opposite faces would give no net viscous contribution from their difference. The author therefore concludes that the Navier–Stokes viscous-force term cannot be obtained if that finite-element equality is enforced. This is the proposed incompatibility between the two constructions: one requires spatial stress increments, while the other has been interpreted as excluding them throughout the fluid domain.

The Author's Argument.

The author's objection is that the stress-increment notation in Figure 13 is routinely used without an explicit comparison with the finite-element equality proposed above. Within the author's interpretation, those increments can be retained only if that equality is relaxed. The author therefore regards the standard derivation as using stresses in a way that is inconsistent with the proposed reading of the symmetry requirement. A related concern is raised for the definition of wall shear and the calculation of lift and drag, where the author considers an additional component to have been omitted. These are arguments about the compatibility of particular constructions; they do not establish that researchers deliberately discard a physical law. The point requiring examination is the relation between local tensor symmetry, the positions at which components are evaluated, and the faces on which the resulting tractions act.

5.3. Proposed Grid Dependence of Fluid Stresses

For the next comparison, suppose that the directional stress increments are retained, as in the standard differential-element treatment [9,41–43]. The author then imposes the selected pairwise equalities on the components shown in Figure 13. With those assumptions stated together, the two relations used in the argument are

$$\begin{cases} \tau_{13} = \tau_{31} \quad \text{(at the lower-left corner)}, \\ \tau_{13} + \dfrac{\partial \tau_{13}}{\partial x_3}\Delta x_3 = \tau_{31} + \dfrac{\partial \tau_{31}}{\partial x_1}\Delta x_1 \quad \text{(at the upper-right corner)}. \end{cases} \tag{37}$$

Combining the two relations in Eq. (37) gives

$$\frac{\partial \tau_{13}}{\partial x_3} = \frac{\partial \tau_{31}}{\partial x_1}\left(\frac{\Delta x_1}{\Delta x_3}\right). \tag{38}$$

For a sufficiently small element, the partial derivatives $\frac{\partial \tau_{13}}{\partial x_3}$ and $\frac{\partial \tau_{31}}{\partial x_1}$ describe local changes in their respective coordinate directions. The author argues that their values should follow from the flow field rather than from an arbitrary choice of element shape. However, the relation in Eq. (38), obtained from the selected pairwise equalities, ties their ratio to $\frac{\Delta x_1}{\Delta x_3}$. On that basis, changing the element aspect ratio changes the relation inferred between the two derivatives. For example, doubling Δx_1 while keeping Δx_3 fixed would double the inferred value of $\frac{\partial \tau_{13}}{\partial x_3}$ if $\frac{\partial \tau_{31}}{\partial x_1}$ were held unchanged. The element could remain small in absolute terms, yet the inferred relation would change. The author interprets this dependence as incompatible with convergence to a unique local stress field. The proposed objection therefore concerns the aspect-ratio constraint introduced by the selected stress equalities, rather than a demonstrated failure of a particular numerical discretisation.

The author concludes that the stated relation would retain an explicit dependence on element aspect ratio even as the element dimensions become small. This differs from the discretisation errors investigated in ordinary CFD grid-convergence studies [54–56], where refinement is used to assess convergence of a numerical solution. In Eq. (38), the proposed dependence is built into the relation between the selected derivatives and does not disappear merely by reducing both dimensions. The distinction is central to the author's argument and should be assessed at the level of the assumed stress comparison.

5.4. The Proposed Conflict with Differential Calculus

The planar Poiseuille expressions in Eq. (36) give the following directional derivatives:

$$\frac{\partial \tau_{13}}{\partial x_3} = \left(\frac{\Delta p}{\Delta x}\right) \text{ and } \frac{\partial \tau_{31}}{\partial x_1} = 0. \tag{39}$$

Using the specified displacement Δx_3, the corresponding first-order expansion for τ'_{13} is

$$\tau'_{13} = \tau_{13} + \frac{\partial \tau_{13}}{\partial x_3}\Delta x_3 = \tau_{13} + \left(\frac{\Delta p}{\Delta x}\right)\Delta x_3, \tag{40}$$

The expansion for τ'_{31} along the specified x_1 displacement is instead

$$\tau'_{31} = \tau_{31} + \frac{\partial \tau_{31}}{\partial x_1}\Delta x_1 = \tau_{31}. \tag{41}$$

Under the construction used above, Eq. (40) includes the increment $\left(\frac{\Delta p}{\Delta x}\right)\Delta x_3$ in τ_{13} when the pressure gradient is nonzero. In contrast, Eq. (41) gives no increment for τ_{31} along the specified x_1 displacement. The difference reflects the directions selected for the two increments: the planar Poiseuille velocity varies with z, while it is independent of x. The author's argument compares these two expressions to examine whether the selected stress-pair construction remains compatible with the imposed symmetry requirement.

At the initial point, the author imposes the complementary equality $\tau_{13} = \tau_{31}$. Comparing Eqs. (40) and (41) then gives unequal primed values when the imposed pressure gradient is nonzero. Under the identification made in the element construction, these values are treated as stresses at the same upper-right location, leading to $\tau'_{13} \neq \tau'_{31}$. The author interprets this result as a conflict between the selected symmetry requirement and differential calculus in planar Poiseuille flow. The conclusion therefore depends on how the two directional expansions are used to identify the final evaluation point. This dependency is essential when assessing whether the apparent contradiction concerns tensor symmetry itself or the spatial comparison used in the derivation.

6. Stokes Flow: A Classical Analytical Solution

Stokes' drag law provides an explicit expression for the resistance experienced by a sphere in a sufficiently slow viscous flow. Its successful application contributed substantially to the acceptance of the classical equations of fluid motion. Stokes' investigation

of internal friction [57] addressed the motion of pendulums and the influence of fluid resistance, while the sphere solution subsequently provided a foundation for viscosity measurements [58]. These applications are valuable because they connect a tractable mathematical solution with quantities that can be measured experimentally. Cartwright [59] also discusses the broader scientific influence of Stokes' law, including its connection with work associated with three Nobel Prizes in Physics and one in Chemistry. The example is therefore important both historically and practically. In the present paper, it offers a configuration in which the expected drag and the absence of transverse lift can be compared with the author's proposed stress interpretation.

In particular, Millikan [60] used a corrected form of Stokes' law in determining the elementary electric charge. This work formed part of the research recognised by the 1923 Nobel Prize in Physics and illustrates the importance of understanding the conditions under which a viscous-drag relation is applied.

Stokes used the symmetric stress formulation in the classical treatment of viscous motion [7]. The agreement of the resulting drag law with appropriate low-Reynolds-number applications therefore reinforced confidence in that description. The present author proposes a different interpretation of the component forces acting on the sphere and examines its consequences for both drag and lift. Because the configuration is symmetric about the flow axis, the transverse resultant should vanish, as discussed by Lautrup [61]. The comparison is consequently a test of the proposed surface-force assignment: any nonzero transverse resultant must be reconciled with the symmetry of the stated flow.

Following Stokes' paper, published in 1851 [57], consider a sphere of radius a moving to the right at speed U. In a frame moving with the sphere, the corresponding problem is a uniform flow approaching the stationary sphere from the right, as illustrated in Figure 14. The analysis assumes steady creeping flow, so the inertial terms are neglected relative to the viscous terms. Under these conditions, the Navier–Stokes equations reduce to the Stokes equations written below:

$$\begin{cases} \nabla p = \mu \nabla^2 \vec{V}, \\ \nabla \cdot \vec{V} = 0. \end{cases} \tag{42}$$

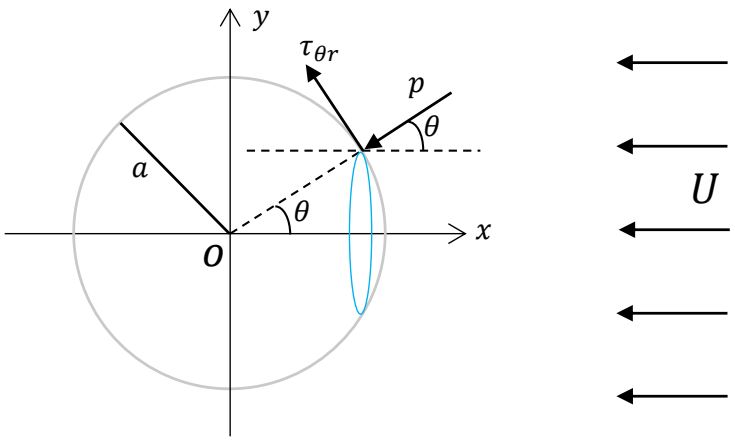


Figure 14. Pressure and tangential viscous traction on the sphere surface.

The flow is axisymmetric about the x axis. It can therefore be described using the radial and polar components shown in Figure 14, with the following boundary conditions at the sphere surface and far from it:

$$\begin{cases} u_r = 0, \quad u_\theta = 0 \quad \text{when } r = a, \\ u_r = -U\cos\theta, \quad u_\theta = U\sin\theta \quad \text{when } r = \infty. \end{cases} \tag{43}$$

Here r denotes the distance from the centre of the sphere to the field point, and θ denotes the angle measured from the x axis in the illustrated meridional plane. The positive angular direction is taken to be anticlockwise in that diagram.

Solving the reduced equations subject to the stated surface and far-field conditions gives the following radial and polar velocity components for the creeping-flow field:

$$\begin{cases} u_r = -U\cos\theta\left(1 - \dfrac{3a}{2r} + \dfrac{a^3}{2r^3}\right), \\ u_\theta = U\sin\theta\left(1 - \dfrac{3a}{4r} - \dfrac{a^3}{4r^3}\right), \end{cases} \tag{44}$$

The associated pressure field is obtained from the same solution and can be written as

$$p = \mu\cos\theta\,\frac{\partial}{\partial r}\left(\frac{\partial^2}{\partial r^2} - \frac{2}{r^2}\right)\left[\frac{1}{4}Ua^2\left(-\frac{2r^2}{a^2} + \frac{3r}{a} - \frac{a}{r}\right)\right] = \frac{3}{2}\mu U\frac{a}{r^2}\cos\theta. \tag{45}$$

Evaluating these expressions at the sphere surface gives the following surface quantities:

$$p|_{r=a} = \frac{3\mu U}{2a}\cos\theta. \tag{46}$$

White and Majdalani [48] and Lautrup [61] give corresponding expressions using the opposite convention for the direction of the incoming flow. Their signs must therefore be interpreted consistently when comparing the surface-force components.

Using the conventional symmetric stress relation in spherical coordinates, the tangential wall shear stress on the sphere is expressed as follows:

$$\tau^{sym}_{\theta r}\Big|_{r=a} = \tau^{sym}_{r\theta}\Big|_{r=a} = \mu\left(\frac{1}{r}\frac{\partial u_r}{\partial\theta} + \frac{\partial u_\theta}{\partial r} - \frac{u_\theta}{r}\right)_{r=a} = \frac{3\mu U}{2a}\sin\theta. \tag{47}$$

Following Stokes [57], with corresponding treatments in White and Majdalani [48] and Lautrup [61], the drag is obtained by integrating the streamwise components of pressure and tangential viscous traction over the sphere. For the geometry and sign convention in Figure 14, the expression is

$$D = -\int_S \tau_{\theta r}|_{r=a}\sin\theta\,dA - \int_S p|_{r=a}\cos\theta\,dA = -4\pi\mu Ua - 2\pi\mu Ua = -6\pi\mu Ua, \tag{48}$$

Here $dA = 2\pi a^2\sin\theta\,d\theta$ is the area of the spherical ring between the polar angles θ and $\theta + d\theta$. The negative sign of D indicates that the force acts in the incoming-flow direction under the selected coordinate convention. Its magnitude is the familiar Stokes drag, $6\pi\mu Ua$. Keeping the sign convention separate from the magnitude avoids ambiguity when comparing formulas written for opposite flow directions.

Using the same pressure p and tangential wall shear stress τ, the manuscript represents the transverse-force calculation by the following integral. The expression is retained here to make the proposed comparison explicit:

$$L = \int_S \tau_{\theta r}|_{r=a}\cos\theta\,dA - \int_S p|_{r=a}\sin\theta\,dA = 0. \tag{49}$$

The stated calculations recover the familiar drag magnitude and a zero transverse resultant. The former agrees with Stokes drag under the creeping-flow assumptions, while the latter is consistent with the symmetry of the configuration. These expected outcomes provide the reference against which the author compares the proposed additional stress contribution.

The author nevertheless regards the force assignment as incomplete under the interpretation introduced in Section 3. In addition to the tangential wall component $\tau_{\theta r}$, the proposed construction assigns the complementary component $\tau_{r\theta}$ as an additional radial

contribution on the sphere surface. This component is shown in red in Figure 15. The author argues that, once it is assigned to that surface, it must be included in the force balance under Newton's third law. The following drag expression therefore retains the original pressure and tangential contributions and adds the proposed radial term. The distinction between a complementary tensor component and the traction on a selected surface is the central interpretive issue in this step, and the result below follows from the assignment stated here:

$$D = -\int_S \tau_{\theta r}|_{r=a} \sin\theta \, dA + \int_S (\tau_{r\theta} - p)|_{r=a} \cos\theta \, dA = -4\pi\mu U a - 2\pi\mu U a = -6\pi\mu U a. \tag{50}$$

Under this proposed construction, the added contribution does not change the streamwise drag resultant. Applying the same assignment in the manuscript's transverse-force calculation, however, gives the following expression for lift:

$$L = \int_S \tau_{\theta r}|_{r=a} \cos\theta \, dA + \int_S (\tau_{r\theta} - p)|_{r=a} \sin\theta \, dA = 4\pi\mu U a. \tag{51}$$

The proposed calculation therefore gives a nonzero lift on the sphere. Such a result is incompatible with the symmetry of the stated creeping-flow configuration. The author interprets this discrepancy as an objection to the application of the symmetric stress tensor under the force construction used here. The conclusion depends specifically on the assignment of the additional stress contribution to the sphere surface, which is the point at issue in the preceding discussion.

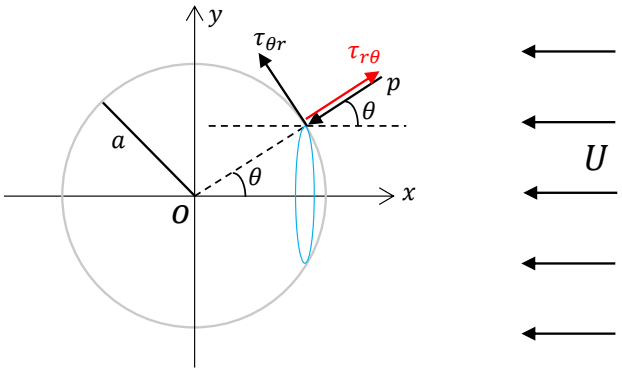


Figure 15. Pressure and stress contributions in the author extquotesingle s proposed sphere-force calculation.

The Author's Argument.

The author identifies two perceived differences between the conventional statement of stress symmetry and its application in surface-force calculations. First, a symmetric constitutive relation may be used to calculate tangential wall shear, while the additional radial contribution proposed here is absent from the resultant-force expression. The sphere calculation is presented as an example of this situation. Second, a wall-shear relation may be written directly in terms of a single normal velocity gradient, without displaying the full tensor expression from which it follows. The author associates the familiar airfoil formulas with this second presentation. In both cases, the concern is that the component assigned as an additional surface force in the present argument is not explicitly included. The author therefore calls for a consistent interpretation of stress indices, surface normals, and force directions before the resultant lift or drag is evaluated. A complete balance must include all actual tractions on the selected surface, and every component used in that balance must have a clearly identified plane of action. The proposed discrepancy is consequently about that identification, rather than simply the presence or absence of a tensor symbol in a final formula.

Within the proposed force construction, the pressure and the added stress contributions produce the nonzero lift in Eq. (51). The author regards this result as inconsistent with the expected symmetry of the physical flow and attributes the discrepancy to the adopted interpretation of the symmetric stress tensor. The calculation is intended to include every force contribution that the author considers necessary under Newton's third law. Accordingly, the subsequent study [17] proposes an asymmetric stress formulation as a way of addressing the discrepancy. This conclusion remains tied to the force assignment used in the present derivation and should be assessed together with that assignment.

7. Rotational Motion of Fluids

Rotating flows provide important examples for understanding fluid motion [62], including the stability of a viscous liquid between rotating cylinders [63]. Rigid-body rotation is also used in explaining the conventional Newtonian stress relation, because its symmetric velocity gradient vanishes [40]. The resulting absence of viscous stress is often described as a stress-free rotating state, although pressure remains present. This section examines the author's question about whether that description can be extended to a configuration that transmits torque under an applied load. The distinction between an unloaded steady rotation and a proposed loaded arrangement is therefore central to the discussion.

7.1. General Rotational Flow and Rigid-Body Rotation

Consider a fluid confined between two concentric cylinders of radii R_1 and R_2, each connected to a separate shaft, as shown in Figure 16. Their angular velocities are denoted by ω_1 and ω_2. Changing these angular velocities changes the velocity distribution in the intervening fluid and provides a direct way to compare differential rotation with the special case of common rigid-body rotation.

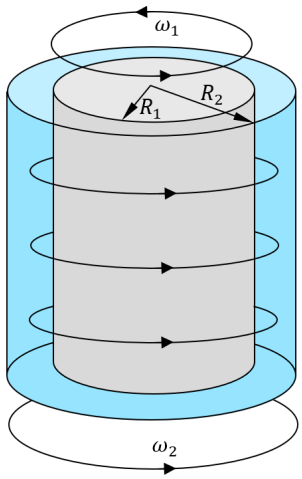


Figure 16. Fluid rotation between concentric cylinders.

For the steady laminar configuration considered here, the azimuthal velocity has the following standard form [48,64], with the constants determined by the prescribed cylinder velocities:

$$\begin{cases} u_\theta = R_1\omega_1 \dfrac{\dfrac{R_2}{r} - \dfrac{r}{R_2}}{\dfrac{R_2}{R_1} - \dfrac{R_1}{R_2}} + R_2\omega_2 \dfrac{\dfrac{r}{R_1} - \dfrac{R_1}{r}}{\dfrac{R_2}{R_1} - \dfrac{R_1}{R_2}}, \\ u_r = 0. \end{cases} \tag{52}$$

The general case of differential rotation is not the principal subject here. Instead, consider the simpler condition $\omega_1 = \omega_2 = \omega$, in which both cylinders have the same

angular velocity. Once the steady state is reached, the intervening fluid rotates with the cylinders as a rigid body. The velocity is then proportional to the radial distance from the axis, and the motion is written as follows:

$$\begin{cases} u_\theta = \omega r, \\ u_r = 0. \end{cases} \tag{53}$$

In cylindrical coordinates, the conventional viscous stress components for the two-dimensional rotational motion considered here are written as

$$\begin{cases} \tau_{rr} = 2\mu \dfrac{\partial u_r}{\partial r}; \quad \tau_{\theta\theta} = 2\mu \left(\dfrac{1}{r} \dfrac{\partial u_\theta}{\partial \theta} + \dfrac{u_r}{r} \right), \\ \tau_{\theta r} = \tau_{r\theta} = \mu \left(\dfrac{1}{r} \dfrac{\partial u_r}{\partial \theta} + \dfrac{\partial u_\theta}{\partial r} - \dfrac{u_\theta}{r} \right). \end{cases} \tag{54}$$

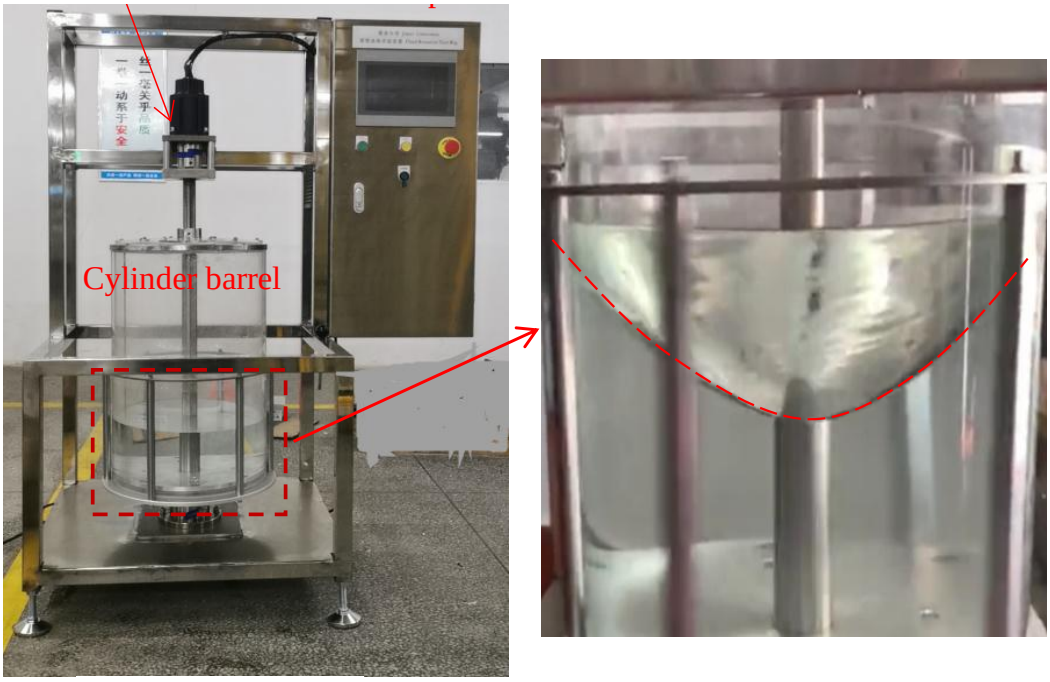
Substituting the rigid-body velocity field into these component expressions gives zero for each viscous stress component:

$$\begin{cases} \tau_{rr} = 0; \quad \tau_{\theta\theta} = 0, \\ \tau_{\theta r} = \tau_{r\theta} = 0. \end{cases} \tag{55}$$

This result agrees with the conventional Newtonian description of rigid-body rotation: the viscous stress vanishes because the motion contains no rate of deformation. Consequently, the viscous stress contributes neither mechanical-energy transfer nor viscous dissipation within that idealised state. The absence of relative sliding between neighbouring fluid particles provides a physical description of the same kinematic condition. The author regards this property as an important motivation for the conventional symmetric constitutive relation, discussed in [40]. A rotating barrel provides a useful example, corresponding to the limiting arrangement in which the inner radius is zero, $R_1 = 0$. The experimental apparatus in Figure 17(a) includes a driving motor and a control panel used to set the target angular speed. During each run, the cylindrical barrel is accelerated towards that target, after which the rotation is maintained at approximately constant speed. The shaft torque and rotational speed are recorded during the process, as shown in Figure 18. Both signals approach steady operating values after the initial acceleration. Small torque variations may be associated with residual speed variations, although their origin cannot be established from the plotted signals alone. The water surface assumes a concave paraboloidal profile, illustrated in Figure 17(b), consistent with the standard rotating-fluid surface relation discussed in [11]. The curvature of that surface does not, by itself, imply continued relative sliding within the final rotating state. The comparison of interest is between the steady motion of the water and the motion of a solid rotating with the same apparatus. It is also important to distinguish the shaft torque measured by the apparatus from the internal viscous dissipation inferred for the water: the measured signal can include the mechanical losses required to maintain rotation of the apparatus. The reported comparison is used below to examine the extent to which the two operating conditions produce similar measured torques.

The absence of relative sliding in ideal rigid-body rotation implies zero Newtonian viscous dissipation within the fluid. To compare the reported rotating-water behaviour with solid rotation, Figure 18 includes measurements obtained using steel discs. The discs were selected to have the same nominal radius and mass as the water used in the comparison. These choices provide a basis for comparison, although equality of mass and outer radius alone does not guarantee identical moments of inertia if the radial mass distributions differ. In particular, the water redistributes as its free surface curves during rotation. The author considers the resulting difference to be small at the speeds used, but the supplied material does not provide a separate measurement of that effect. The torque comparisons at the reported speeds are listed in Table 1, where the magnitudes of the tabulated relative differences are below 1%. The author interprets this close agreement as consistent with

approximately rigid rotation of the water once the steady operating state is reached. The comparison supports a discussion of similar measured shaft loads, while the precision with which internal fluid losses can be distinguished depends on the measurement uncertainty and the apparatus losses. Those details are not established by the torque differences alone. The relative difference is calculated as $100(T_{\text{water}} - T_{\text{solid}})/T_{\text{solid}}$, so the negative tabulated values indicate slightly smaller measured torques for water at the corresponding speeds.



(a) Rotating test rig (b) Revolving surface of the fluid

Figure 17. Rotating-barrel apparatus and water-surface profile (courtesy of Jimei University, China).

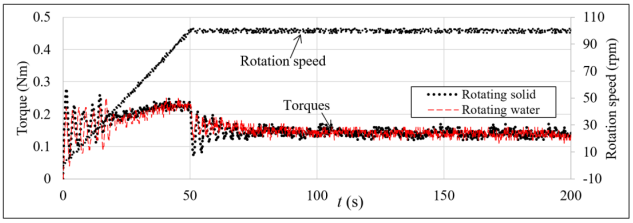


Figure 18. Measured shaft torques for rotating solid discs and water (data from Jimei University, China).

Table 1. Measured torques at different rotational speeds.

Rotation speed (rpm)	Torque (N m)		Relative difference (%)
	Rotating solid	Rotating water	
100	0.1406	0.140	-0.43
50	0.121	0.120	-0.83
10	0.0822	0.0821	-0.12
5	0.0777	0.0772	-0.64

7.2. Stress-Free Rigid Rotation: Examining the Assumptions

The rotating-barrel comparison raises a further question in the author's argument: does the absence of viscous dissipation necessarily imply that every relevant stress contribution must vanish? The following proposed configuration is used to distinguish the

transmission of torque from the conversion of mechanical energy into heat within the rotating material. It is presented as a physical argument concerning the imposed loading conditions, rather than as an additional measured data set comparable with Figure 18 and Table 1.

Consider a concentric-cylinder arrangement in which the intervening material is pitch rather than water or oil. Pitch has a very large viscosity, of the order of 10^7–10^8 Pa s in the conditions discussed here, compared with approximately 10^{-3} Pa s for water. The dark-grey region in Figure 19 represents pitch filling the space between the cylinders. Although it appears solid over short observation periods, its ability to flow slowly is demonstrated by the well-known pitch-drop experiment [65]. The proposed example uses this contrast between apparent rigidity and slow flow to discuss torque transmission during rotation.

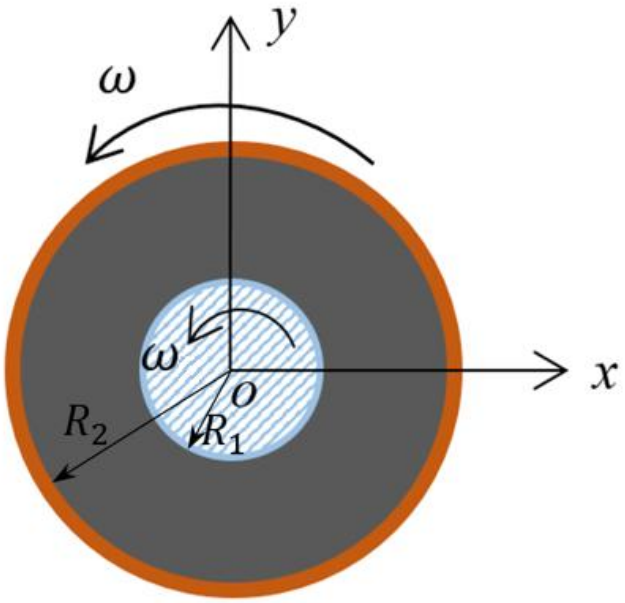


Figure 19. Proposed pitch-filled cylinder arrangement for discussing torque transmission.

In the proposed arrangement, the outer cylinder is connected to a driving motor and the inner cylinder to a driven shaft. When the outer cylinder rotates, the intervening pitch transmits motion towards the inner cylinder. The argument assumes that the two cylinders and the pitch rotate together at the same angular speed, so that the pitch remains effectively rigid over the period considered. This assumed state is the basis of the comparison: the question is whether torque can be transmitted through the material while the motion is described as rigid rotation, rather than whether an additional velocity profile has been measured experimentally.

In an ideal arrangement without shaft friction or other resisting loads, steady rotation would require no continuing torque to overcome such losses. The author's proposed example then assigns no torque-transmitting shear stress to the pitch. A practical apparatus, however, can have friction at its shafts, bearings, and other mechanical interfaces, so the loaded case must be considered separately.

Suppose that friction applies a resisting torque to the inner shaft. Maintaining steady rotation then requires the motor to supply a corresponding driving torque at the outer cylinder. Under the proposed operating condition, the outer cylinder, pitch, and inner cylinder all rotate at an approximately constant angular speed. Mechanical energy supplied by the motor is transmitted through the intervening material to the loaded shaft and is ultimately dissipated as heat at the resisting interface. The author's argument distinguishes this external dissipation from any dissipation occurring within the pitch itself. The question is therefore how the internal stresses required for torque transmission should be described under the assumed nearly rigid motion.

The proposed argument assumes that relative sliding within the pitch is negligible over the observation period. With that assumption, the author asks whether all torque-transmitting stresses could nevertheless be zero. A resisting moment on the inner shaft must be balanced by a transmitted moment if the shaft is to continue rotating steadily. If every relevant shear traction within the pitch vanished, the stated arrangement would provide no mechanism for transmitting that moment from the outer cylinder to the inner one. The author therefore infers that nonzero stress must exist under the loaded condition. This inference concerns the compatibility of the loading and the assumed motion. The constitutive description of pitch, the observation time, and the distinction between exactly rigid motion and very slow deformation remain essential to interpreting the example.

Under the assumed absence of relative sliding, the author separates the transfer of mechanical energy through the pitch from its dissipation at the loaded shaft. The proposed conclusion is that zero internal dissipation does not, by itself, describe every possible mechanism of stress transmission in a rotating material. Whether the chosen material and loading can sustain the assumed motion must be specified before that conclusion is extended to a Newtonian fluid. The example is therefore used to question the physical interpretation of the rotating state, with particular emphasis on the imposed load and the time scale over which the material appears rigid.

8. Energy Transfer and Dissipation in Compressible Flows

To examine mechanical-energy transfer and viscous dissipation, consider the work done by the stress components on the top and bottom faces of the element in Figure 20. Combining each component with its corresponding velocity gives the following contribution per unit volume. The standard derivation is discussed in [47].

$$\frac{\partial(u_1\tau_{13})}{\partial x_3} + \frac{\partial(u_2\tau_{23})}{\partial x_3} + \frac{\partial(u_3\tau_{33})}{\partial x_3}. \tag{56}$$

In the sign convention used here, the displayed velocities and tractions have matching directions on the top face and opposing directions on the bottom face. Their difference gives the net contribution from that pair of faces.

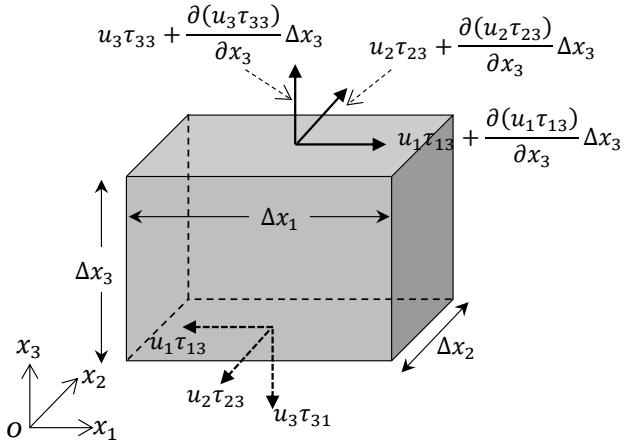


Figure 20. Viscous energy transfer and dissipation in a fluid element.

Adding the corresponding contributions from the left and right faces and from the front and rear faces gives the complete viscous stress-power expression for the element:

$$\begin{aligned}&\frac{\partial(u_1\tau_{11})}{\partial x_1} + \frac{\partial(u_2\tau_{21})}{\partial x_1} + \frac{\partial(u_3\tau_{31})}{\partial x_1} + \frac{\partial(u_1\tau_{12})}{\partial x_2} + \frac{\partial(u_2\tau_{22})}{\partial x_2} + \frac{\partial(u_3\tau_{32})}{\partial x_2}\\ &+ \frac{\partial(u_1\tau_{13})}{\partial x_3} + \frac{\partial(u_2\tau_{23})}{\partial x_3} + \frac{\partial(u_3\tau_{33})}{\partial x_3} = \frac{\partial(u_i\tau_{ij})}{\partial x_j}.\end{aligned} \tag{57}$$

Using the Einstein summation convention to collect the component contributions, the final expression can also be rearranged into the following form:

$$\frac{\partial(u_i\tau_{ij})}{\partial x_j} = \tau_{ij}\frac{\partial u_i}{\partial x_j} + u_i\frac{\partial \tau_{ij}}{\partial x_j}. \tag{58}$$

The first term on the right-hand side is the conventional viscous dissipation function, defined here as

$$\Phi = \tau_{ij}\frac{\partial u_i}{\partial x_j}. \tag{59}$$

Substituting the symmetric stress components from Eq. (16) gives the expanded expression for the dissipation function:

$$\Phi = \mu\left\{\begin{array}{l} 2\left[\left(\frac{\partial u}{\partial x}\right)^2 + \left(\frac{\partial v}{\partial y}\right)^2 + \left(\frac{\partial w}{\partial z}\right)^2\right] \\ + \left(\frac{\partial u}{\partial y} + \frac{\partial v}{\partial x}\right)^2 + \left(\frac{\partial w}{\partial y} + \frac{\partial v}{\partial z}\right)^2 \\ + \left(\frac{\partial u}{\partial z} + \frac{\partial w}{\partial x}\right)^2 - \frac{2}{3}\left(\frac{\partial u}{\partial x} + \frac{\partial v}{\partial y} + \frac{\partial w}{\partial z}\right)^2 \end{array}\right\}. \tag{60}$$

This expression is given in standard treatments [12,48]. The negative contribution in its final term follows from the imposed relation $\lambda = -2\mu/3$, rather than from stress symmetry alone. For incompressible motion, the velocity divergence vanishes and this term makes no contribution. For compressible motion, it must be interpreted together with the remaining terms in the quadratic expression. The author's concern is whether its role is consistent with the physical dissipation mechanisms expected under the particular flow conditions.

High-speed compressible flows can involve several mechanisms of mechanical-energy conversion, transport, and dissipation, including those discussed in [66,67]. Their importance depends on the thermodynamic state, flow gradients, material properties, and relevant boundary conditions. For the comparison developed below, the mechanisms motivating the author's question can be described as follows:

1) Compressibility and shocks: when the flow conditions permit shock formation, abrupt changes in pressure, density, and temperature are associated with irreversible thermodynamic processes. Dilatational motion can also contribute to viscous dissipation when the material's bulk viscosity is nonzero. These mechanisms should be distinguished from compressibility considered solely as a change in density.

2) Viscous dissipation: temperature and pressure variations can alter the transport properties and gradients that determine conversion of mechanical energy into heat. The resulting change in dissipation depends on those properties and gradients, rather than following from a universal increase associated with compressibility alone. 3) Turbulent energy transfer: compressible turbulence includes density fluctuations, pressure–dilatation interactions, and changes in the distribution of kinetic and internal energy. These processes may modify the balance between transfer and irreversible dissipation. 4) Acoustic transport and attenuation: pressure fluctuations can generate sound waves that carry energy away from a region. Subsequent attenuation can convert part of that acoustic energy into heat. These mechanisms provide distinct contexts for interpreting the local viscous dissipation function used in the following calculation.

For the specific constitutive relation used here, the dissipation function can be rearranged to display its nonnegative quadratic contributions more directly. The resulting expression is

$$\Phi = \mu \left\{ \begin{array}{l} \frac{2}{3}\left[\left(\frac{\partial u}{\partial x} - \frac{\partial v}{\partial y} \right)^2 + \left(\frac{\partial v}{\partial y} - \frac{\partial w}{\partial z} \right)^2 + \left(\frac{\partial u}{\partial x} - \frac{\partial w}{\partial z} \right)^2 \right] \\ + \left(\frac{\partial u}{\partial y} + \frac{\partial v}{\partial x} \right)^2 + \left(\frac{\partial w}{\partial y} + \frac{\partial v}{\partial z} \right)^2 \\ + \left(\frac{\partial u}{\partial z} + \frac{\partial w}{\partial x} \right)^2 \end{array} \right\}. \tag{61}$$

For nonnegative dynamic viscosity, the displayed quadratic form is nonnegative. It therefore does not predict negative viscous dissipation. Positive values represent irreversible conversion of mechanical energy into internal energy, whereas zero values identify motions for which this constitutive model predicts no viscous conversion.

Although Eq. (61) is nonnegative, it need not be strictly positive for every compressible motion. Consider the following particular velocity-gradient field:

$$\frac{\partial u}{\partial x} = \frac{\partial v}{\partial y} = \frac{\partial w}{\partial z} = \varepsilon \neq 0 \quad \text{and} \quad \frac{\partial u_i}{\partial x_j} = 0 \quad \text{for } i \neq j. \tag{62}$$

The specified field describes isotropic dilatation without a shear contribution. Its velocity divergence is nonzero, as shown by

$$\nabla \cdot \vec{V} = \frac{\partial u}{\partial x} + \frac{\partial v}{\partial y} + \frac{\partial w}{\partial z} = 3\varepsilon \neq 0. \tag{63}$$

Nevertheless, substitution into the selected dissipation function gives zero for this particular motion:

$$\Phi = 0. \tag{64}$$

The calculation therefore gives zero viscous dissipation for the specified dilatational motion when Stokes' hypothesis is imposed, while the general quadratic expression remains nonnegative. The author regards this result as a reason to examine carefully how compressibility and the second viscosity coefficient are represented in the model. In particular, the example distinguishes the algebraic consequences of the chosen coefficient relation from the broader energy-conversion mechanisms listed above. The conclusion drawn in this investigation is that the assumed relation deserves further scrutiny when the dissipation of compressible flows is interpreted. Whether that concern requires a different bulk-viscosity model, a different stress formulation, or a narrower statement of the physical conditions must be assessed from the constitutive assumptions themselves.

9. Conclusions

The Navier–Stokes equations provide the conventional governing framework for Newtonian viscous flow under the assumptions of classical continuum mechanics. Within that framework, the symmetric stress relation is associated with angular-momentum balance and gives zero viscous stress for exact rigid-body rotation. This investigation has examined the author's proposed objections to the interpretation of those statements in several familiar flow configurations. The discussion combines component calculations with a reported comparison of rotating water and solid discs; it does not establish a general experimental replacement for the conventional constitutive model. The conclusions drawn within the author's argument are summarised below, with the underlying assumptions retained as part of each claim.

1) The earlier discussion of Couette flow [15] questions the interpretation of a complementary shear component when no velocity component is present in its force direction. The planar Poiseuille example extends that question by displaying the corresponding velocity distribution and shear components explicitly.

2) Applying the author's selected equalities across different faces of an element leads to a uniform-stress inference. If that inference is imposed throughout the domain, the spatial stress increments needed to construct the viscous-force term vanish. The proposed objection to the momentum-equation derivation depends on this face-to-face identification.

3) Retaining directional stress increments while imposing the selected pairwise equalities gives a relation containing the element aspect ratio. The author interprets this as a persistent grid dependence that differs from ordinary discretisation error. The conclusion therefore concerns the imposed comparison between derivatives rather than a demonstrated convergence failure of a specified CFD method.

4) In planar Poiseuille flow, the author's comparison of increments in different directions produces unequal primed stress values. This is interpreted as an inconsistency between the selected symmetry construction and differential calculus. Assessment of that claim requires careful identification of the spatial point associated with each expanded component.

5) For Stokes flow past a sphere, adding the proposed radial contribution leaves the stated drag unchanged but produces a nonzero transverse resultant. Since the physical configuration is symmetric, this result indicates a discrepancy in the proposed description. The author attributes it to the symmetric stress interpretation, while the assignment of the component to the sphere surface remains the critical step in the argument.

6) The reported rotating-water and solid-disc torques differ by less than 1% in the tabulated comparison. A separate proposed pitch-cylinder example is used to distinguish torque transmission from internal dissipation. The conclusions for that example depend on the material model, the applied load, and the distinction between exact rigid rotation and deformation too slow to be resolved over the observation period.

7) Stokes' hypothesis assigns $\lambda = -2\mu/3$ and gives zero dissipation for the particular isotropic dilatation examined here. The author regards this as a reason to scrutinise the treatment of compressibility. The result concerns the selected bulk-viscosity restriction and should be distinguished from the more general requirement that the stress tensor be symmetric.

This first part of the investigation sets out the author's proposed difficulties with the interpretation of the SST and identifies the component assignments and constitutive assumptions on which they depend. The aim is to make the arguments sufficiently explicit for detailed examination, rather than to rely solely on the historical acceptance or practical success of a formulation. The subsequent study [17] proposes an asymmetric stress tensor and considers how that description would address the issues presented here. It also discusses why the conventional equations have remained successful in many applications and what would change under the proposed alternative. The central question for further assessment is whether each claimed discrepancy follows from the constitutive symmetry condition itself or from the additional assumptions introduced when that condition is applied to a particular element, surface, or material.

Acknowledgments

The author thanks Prof. Hui Li of Jimei University, China, for constructing the test apparatus, conducting the comparison experiments involving rigidly rotating water and rotating solid discs, and providing the experimental results used in the present discussion.

Competing Interests

The author declares no competing interests.

Data Availability

The experimental comparisons reported in this manuscript are presented in Figure 18 and Table 1. The supplied manuscript does not include the original instrument records or the detailed processing procedures used to obtain these results.

Funding

This research received no external funding.

References

[1] Anderson, J. D., Jr. (1997). *A History of Aerodynamics and Its Impact on Flying Machines*. Cambridge University Press.
[2] Newton, I. (1846). *Newton's Principia: The Mathematical Principles of Natural Philosophy* (A. Motte, Trans.; N. W. Chittenden, Ed.). Daniel Adee.
[3] Simón Calero, J. (2008). *The Genesis of Fluid Mechanics, 1640–1780*. Springer.
[4] Darrigol, O. (2002). Between hydrodynamics and elasticity theory: The first five births of the Navier–Stokes equation. *Archive for History of Exact Sciences*, *56*(2), 95–150.
[5] Bistafa, S. R. (2024). 200 years of the Navier–Stokes equation. *Revista Brasileira de Ensino de Física*, *46*, Article e20230398.
[6] Masuda, S. (2012). The study of mathematical history on the equations of Navier–Stokes and Boltzmann as the microscopically-descriptive hydrodynamic equations. *RIMS Kôkyûroku*, *1776*, 75–90.
[7] Stokes, G. G. (1845). On the theories of the internal friction of fluids in motion, and of the equilibrium and motion of elastic solids. *Transactions of the Cambridge Philosophical Society*, *8*, 287–319.
[8] Anderson, J. D., Jr. (2011). *Fundamentals of Aerodynamics* (5th ed.). McGraw-Hill.
[9] Bertin, J. J., & Cummings, R. M. (2013). *Aerodynamics for Engineers* (6th ed.). Pearson.
[10] White, F. M. (2009). *Fluid Mechanics*. McGraw-Hill.
[11] Kundu, P. K., Cohen, I. M., Dowling, D. R., & Capecelatro, J. (2025). *Fluid Mechanics* (7th ed.). Academic Press.
[12] Schlichting, H., & Gersten, K. (2017). *Boundary-Layer Theory* (9th ed.). Springer.
[13] Hibbeler, R. C. (2021). *Fluid Mechanics in SI Units* (2nd ed.). Pearson.
[14] Le Méhauté, B. (1976). *An Introduction to Hydrodynamics and Water Waves*. Springer-Verlag.
[15] Sheng, W. (2020). A revisit of Navier–Stokes equation. *European Journal of Mechanics—B/Fluids*, *80*, 60–71.
[16] Natarajan, G., & Natarajan, M. (2021). Critique on "A revisit of Navier–Stokes equation." *European Journal of Mechanics—B/Fluids*, *85*, 21–23.
[17] Sheng, W. (2026). *A quest to fluid stress tensor, part II: Can we solve the conflicts?* [Report]. Zenodo. https://zenodo.org/records/21638668
[18] Luo, J. (2024). More considerations about the symmetry of the stress tensor of fluids. *The Journal of Chemical Physics*, *161*(4), Article 044112.
[19] Condiff, D. W., & Dahler, J. S. (1964). Fluid mechanical aspects of antisymmetric stress. *The Physics of Fluids*, *7*(6), 842–854.
[20] Aero, E. L., Bulygin, A. N., & Kuvshinskii, E. V. (1965). Asymmetric hydromechanics. *Journal of Applied Mathematics and Mechanics*, *29*(2), 333–346.
[21] Listrov, A. T. (1967). Model of a viscous fluid with an antisymmetric stress tensor. *Journal of Applied Mathematics and Mechanics*, *31*(1), 115–119.
[22] Van D'en, N., & Listrov, A. T. (1967). Nonisothermal model of asymmetric fluids. *Fluid Dynamics*, *2*(5), 87–89.
[23] Lilly, D. K. (1967). The representation of small-scale turbulence in numerical simulation experiments. In *Proceedings of the IBM Scientific Computing Symposium on Environmental Sciences* (pp. 195–210). IBM.
[24] Kim, J., & Leonard, A. (2024). The early days and rise of turbulence simulation. *Annual Review of Fluid Mechanics*, *56*, 21–44.
[25] Saffman, P. G. (1970). A model for inhomogeneous turbulent flow. *Proceedings of the Royal Society of London. Series A, Mathematical and Physical Sciences*, *317*(1530), 417–433.
[26] Hanjalić, K., & Launder, B. E. (1972). A Reynolds stress model of turbulence and its application to thin shear flows. *Journal of Fluid Mechanics*, *52*(4), 609–638.
[27] Launder, B. E., & Spalding, D. B. (1974). The numerical computation of turbulent flows. *Computer Methods in Applied Mechanics and Engineering*, *3*(2), 269–289.
[28] Wilcox, D. C. (2006). *Turbulence Modeling for CFD* (3rd ed.). DCW Industries.
[29] Duraisamy, K., Iaccarino, G., & Xiao, H. (2019). Turbulence modeling in the age of data. *Annual Review of Fluid Mechanics*, *51*, 357–377.
[30] Davidson, L. (2019). *Fluid mechanics, turbulent flow and turbulence modeling* [Course textbook]. Chalmers University of Technology.
[31] Durbin, P. A. (2018). Some recent developments in turbulence closure modeling. *Annual Review of Fluid Mechanics*, *50*, 77–103.
[32] Rodi, W. (2017). Turbulence modeling and simulation in hydraulics: A historical review. *Journal of Hydraulic Engineering*, *143*(5), Article 03117001.
[33] Fernandes, R., Ricklick, M., Prasad, A., & Pai, Y. (2017). Benchmarking Reynolds averaged Navier–Stokes turbulence models in internal pin fin channels. *Journal of Thermophysics and Heat Transfer*, *31*(4), 976–982.
[34] Aftab, S. M. A., Mohd Rafie, A. S., Razak, N. A., & Ahmad, K. A. (2016). Turbulence model selection for low Reynolds number flows. *PLOS ONE*, *11*(4), Article e0153755.
[35] George, W. K. (2013). *Lectures in Turbulence for the 21st Century* [Lecture notes]. https://www.turbulence-online.com/Publications/Lecture_Notes/Turbulence_Lille/TB_16January2013.pdf
[36] Menter, F. R. (2009). Review of the shear-stress transport turbulence model experience from an industrial perspective. *International Journal of Computational Fluid Dynamics*, *23*(4), 305–316.
[37] Ramm, A. G. (2023). *Analysis of the Navier–Stokes Problem: Solution of a Millennium Problem* (2nd ed.). Springer.

[38] Slotnick, J. P., Khodadoust, A., Alonso, J., Darmofal, D., Gropp, W., Lurie, E., & Mavriplis, D. J. (2014). *CFD vision 2030 study: A path to revolutionary computational aerosciences* (NASA/CR-2014-218178). National Aeronautics and Space Administration. https://ntrs.nasa.gov/citations/20140003093

[39] Teschner, T.-R. (n.d.). *The 6 biggest and unsolved challenges in CFD*. CFD University. Retrieved June 12, 2025, from https://cfd.university/blog/the-6-biggest-and-unoslved-challenges-in-cfd/

[40] Newman, J. N. (2017). *Marine Hydrodynamics* (40th anniversary ed.). MIT Press.

[41] Anderson, J. D., Jr. (2017). *Fundamentals of Aerodynamics* (6th ed.). McGraw-Hill Education.

[42] Houghton, E. L., Carpenter, P. W., Collicott, S. H., & Valentine, D. T. (2017). *Aerodynamics for Engineering Students* (7th ed.). Butterworth-Heinemann.

[43] Çengel, Y. A., & Cimbala, J. M. (2018). *Fluid Mechanics: Fundamentals and Applications* (4th ed.). McGraw-Hill Education.

[44] Soldati, A., & Marchioli, C. (2024). *Fluid Mechanics for Mechanical Engineers*. Springer.

[45] Potter, M. C., & Wiggert, D. C. (2025). *Applied Fluid Mechanics* (6th ed.). Springer.

[46] Bar-Meir, G. (2022). *Basics of Fluid Mechanics*. Potto Project. https://zenodo.org/records/6462400

[47] Anderson, J. D., Jr., & Cadou, C. P. (2024). *Fundamentals of Aerodynamics* (7th ed.). McGraw Hill.

[48] White, F. M., & Majdalani, J. (2022). *Viscous Fluid Flow* (4th ed.). McGraw Hill.

[49] Karim, S. M., & Rosenhead, L. (1952). The second coefficient of viscosity of liquids and gases. *Reviews of Modern Physics*, *24*(2), 108–116.

[50] Witherden, F. D., & Jameson, A. (2017). Future directions of computational fluid dynamics. In *23rd AIAA Computational Fluid Dynamics Conference* (AIAA Paper 2017-3791). American Institute of Aeronautics and Astronautics.

[51] Spalart, P. R., & Venkatakrishnan, V. (2016). On the role and challenges of CFD in the aerospace industry. *The Aeronautical Journal*, *120*(1223), 209–232.

[52] Sheng, W., & Aggidis, G. (2022). *Fundamentals of Wave Energy Conversions: The Dynamics of the Wave-Structure Interactions and Wave Energy Optimisation*. Eliva Press.

[53] American Wood Council. (2007). *Beam Design Formulas With Shear and Moment Diagrams* (Design Aid No. 6). American Forest & Paper Association. https://engineering.purdue.edu/~ce474/Docs/DA6-BeamFormulas.pdf

[54] Ali, M. S. M., Doolan, C. J., & Wheatley, V. (2009). Grid convergence study for a two-dimensional simulation of flow around a square cylinder at a low Reynolds number. In *Proceedings of the seventh international conference on CFD in the minerals and process industries* (pp. 1–6). CSIRO.

[55] Sadrehaghighi, I. (2023). *CFD simulation & guidelines* [Technical report]. ResearchGate. https://www.researchgate.net/publication/368511517_CFD_Simulation_Guidelines

[56] Hajgató, G., Gyires-Tóth, B., & Paál, G. (2019). Accelerating convergence of fluid dynamics simulations with convolutional neural networks. *Periodica Polytechnica Mechanical Engineering*, *63*(3), 230–239.

[57] Stokes, G. G. (1851). On the effect of the internal friction of fluids on the motion of pendulums. *Transactions of the Cambridge Philosophical Society*, *9*, 8–106.

[58] Sutterby, J. L. (1973). Falling sphere viscometer. *Journal of Physics E: Scientific Instruments*, *6*(10), 1001–1005.

[59] Cartwright, J. H. E. (2020). Stokes' law, viscometry, and the Stokes falling sphere clock. *Philosophical Transactions of the Royal Society A: Mathematical, Physical and Engineering Sciences*, *378*(2179), Article 20200214.

[60] Millikan, R. A. (1910). The isolation of an ion, a precision measurement of its charge, and the correction of Stokes's law. *Science*, *32*(822), 436–448.

[61] Lautrup, B. (2005). *Physics of Continuous Matter: Exotic and Everyday Phenomena in the Macroscopic World*. IOP Publishing.

[62] Donnelly, R. J. (1991). Taylor–Couette flow: The early days. *Physics Today*, *44*(11), 32–39.

[63] Taylor, G. I. (1923). Stability of a viscous liquid contained between two rotating cylinders. *Philosophical Transactions of the Royal Society of London. Series A, Containing Papers of a Mathematical or Physical Character*, *223*(605–615), 289–343.

[64] Landau, L. D., & Lifshitz, E. M. (1987). *Fluid Mechanics* (J. B. Sykes & W. H. Reid, Trans.; 2nd ed.). Pergamon Press.

[65] Edgeworth, R., Dalton, B. J., & Parnell, T. (1984). The pitch drop experiment. *European Journal of Physics*, *5*(4), 198–200.

[66] Dimotakis, E., & Candler, G. V. (2014). *Energy Transformation, Transfer, and Release Dynamics in High-Speed Turbulent Flows*. https://community.apan.org/cfs-file/__key/telligent-evolution-components-attachments/13-7784-00-00-00-13-54-76/Dimotakis_2D00_Candler.pdf

[67] Yang, X., Xiao, G., Du, Y., Liu, L., Wei, D., & Gui, Y. (2021). Heat transfer with interface effects in high-enthalpy and high-speed flow: Modelling review and recent progress. *Applied Thermal Engineering*, *195*, Article 116721.